NBSIR 87-3647

Microstructural Evaluation of Explosion Bulge Tested HSLA-80 Plates

M. J. Crooks
L. C. Smith
R. C. Reno

U.S. DEPARTMENT OF COMMERCE
National Bureau of Standards
Institute for Materials Science and Engineering
Fracture and Deformation Division
Gaithersburg, MD 20899

October 1987

Sponsored by
David Taylor Naval Ship Research & Development Center
Annapolis, MD 21402

NBSIR 87-3647

MICROSTRUCTURAL EVALUATION OF EXPLOSION BULGE TESTED HSLA-80 PLATES

M. J. Crooks
L. C. Smith
R. C. Reno

U.S. DEPARTMENT OF COMMERCE
National Bureau of Standards
Institute for Materials Science and Engineering
Fracture and Deformation Division
Gaithersburg, MD 20899

October 1987

Sponsored by
David Taylor Naval Ship Research & Development Center
Annapolis, MD 21402

U.S. DEPARTMENT OF COMMERCE, Clarence J. Brown, *Acting Secretary*
NATIONAL BUREAU OF STANDARDS, Ernest Ambler, *Director*

Administrative Information

The investigation reported herein was funded by the Surface Ship and Technology Block Program sponsored by the Materials Block Program (DTNSRDC Code 012.5) and funded under Program Element 62234N, Task Area RS-34-S50, Work Unit 1-2803-117-13, FY87. The effort was monitored by Mr. E.J. Czyryca, David Taylor Naval Ship R&D Center (code 2814).

MICROSTRUCTURAL EVALUATION OF EXPLOSION BULGE TESTED HSLA-80 PLATES

M. J. Crooks, L. C. Smith, and R. C. Reno

SUMMARY

This work was undertaken to examine the microstructures of some HSLA-80 plates. The ultimate aim was to establish microstructural and chemical bases for variability in mechanical properties, in particular, behavior in explosion bulge tests. Steel chemistries, inclusion contents, ferrite microstructures, crystallographic textures and strain-aging responses were considered. Inclusion contents are consistently low in these steels, but elongated sulfides and large, globular oxy-sulfides are occasionally found. The microstructure can be fine-grained polygonal ferrite or acicular ferrite; it can vary through the thickness of the plate. The best combinations of strength and toughness are found in the plates with polygonal ferrite. The texture in these plates is generally weak. In thinner gage plates, there can be a tendency to a {111} <110> texture, which is desirable for strength and toughness. The one variable that clearly distinguishes between plates that passed the bulge test and those that failed is the ratio of aluminum to nitrogen in the steel. For plates that passed the weight percent ratio, Al/N is 4 or greater. In plates with lower Al/N values, the embrittling effects of interstitial nitrogen, which could be present in the heat affected zones of these specimens, is likely responsible for failure in the bulge test. We did not find evidence of strain aging due to nitrogen in the plates as we received them.

BACKGROUND

One of the problems in the use of A710 Grade A Class 3 or HSLA-80 steels has been failure in the explosion bulge test. Plates have been heat treated to meet the requirements for mechanical properties and are otherwise within specifications for this grade, but some plates pass and others fail the explosion bulge test. Response to heat treating is also not always consistent. This work was undertaken to establish microstructural and chemical bases for this variability.

In June 1986, we received broken dynamic tear specimens from a set of HSLA-80 plates which were being evaluated. The identities of those samples and some of the reported mechanical properties of the parent plates are listed in Table I. It is indicated there whether the plate passed or failed the explosion bulge test; the number of shots and the reduction in thickness in the test are

also given. The property data are from a listing that was given to us[1]; they were not measured as part of this work. The chemistries of these steels had been determined earlier[2] and are given in Table II. (Throughout this report, data will be grouped by plate thickness.)

Only three of the plates in this collection, FZF, GES, and GBD, passed the explosion bulge test. One additional plate, GBC, had been heat treated a second time and then passed the test. There are no correlations that we have been able to discover between any of the reported mechanical properties and bulge test results. However, there is an intersting observation that the plates with high Al/N ratios pass the test.[3] Steels with Al/N greater than 4 pass; plate GBC, with Al/N of 3.8, could be processed to pass.

With the exception of plate GES, all of these steels have moderate to high nitrogen contents, which are typical of electric furnace steels. While there is enough nitride-forming alloying, Cb and Al, to remove the nitrogen from interstitial solid solution, it has been shown in other structural grades that strain aging due to mobile nitrogen can occur.[4] There is at least the possibility that variable explosion bulge test results might be due to this mechanism: the test involves deformation, unloading and holding at room temperature for extended period of time (more than a few minutes), then further deformation. Low Al/N values are not inconsistent with mobile nitrogen being present. Since it is a difficult quantity to measure, we examined the strain aging behavior of selected plates of HSLA-80.

In aluminum-killed or fine-grained steels, aluminum-nitride precipitates affect the austenite microstructure during slab reheat and rolling to plate. If the reheat temperature is low enough, so that a sufficient amount of small AlN precipitates are in the slab, then austenite grain growth is inhibited.[5] In steels with Cb, Cb(C,N) precipitates have the same effect and they also inhibit recrystallization during rolling.[6] The interactions between these elements have not been entirely clarified yet and they certainly depend upon the specific details of processing. We cannot determine what the austenite microstructure was at the end of plate rolling, particularly since these steels have been heat treated. However, we have examined the microstructures in the final products, and these should reflect some aspects of the parent-austenite microstructures.

Aside from the aluminum and nitrogen contents, the A710 chemistry has enough alloying to allow the formation of acicular ferrite in commercial production.[7] This is more likely if the austenite grain size is large. Since the typical microstructure is often taken to be mostly polygonal ferrite, variability in mechanical properties might be attributed to variability in ferrite morphology. This has been considered in this work as well.

Another aspect of the microstructure that is important to the behavior of steels is the inclusion content. All of the steels in this study have been desulfurized, but not all of them have been calcium treated, as indicated in Table II. Differences in inclusion shape are expected, particularly in GAG and GES, the steels without calcium additions. If steelmaking practices are

poor, calcium treated steels, even with low sulfur contents, can have large volume fractions of inclusions and the inclusions themselves may be large. These are generally detrimental. For these reasons, the inclusion contents, sizes and morphologies have been examined.

Another aspect of microstructure that affects mechanical properties is crystallographic texture. Particularly under states of multiaxial loading, as in bulge tests, differences in the texture or orientation of grains in a plate can lead to very different responses to loading.[8] We have characterized the texture of several plates in terms of an orientation distribution function that can be deduced from diffraction pole figures. We chose to use neutrons to generate the pole figures because the high penetration power of neutrons ensures that we observe the bulk texture in plates.

EXPERIMENTAL PROCEDURE

Metallography

Samples for metallographic examination were taken from all of the dynamic tear specimens. The plane of polish includes the rolling and through-thickness directions, Figure 1a. All grinding and polishing was done by hand. All samples were examined in the as-polished condition. The morphology and distribution of inclusions in each of the samples were noted.

For examination with light microscopy, the samples were etched in 2% nital. Most samples were suitably etched after 15 to 20 seconds. To examine the carbides in the scanning electron microscope, some samples were repolished then lightly etched in picral and HCl (a couple of drops of HCl in about 50 ml of picral). The samples were immersed for about 12 seconds. Further etching was necessary for one sample; it was etched in picral for 1 minute.

The elemental make-up of inclusions was determined with energy dispersive x-ray spectroscopy. We examined five specimens with different inclusion morphologies. For each specimen, we determined which elements were present in several inclusions and produced some x-ray dot maps to show the physical distribution of elements.

Strain Aging Tests

Six samples for strain aging tests were taken, two from each of three dynamic tear specimens, FZF17, GEA20, and GCM84. The specimen geometry and orientation are shown schematically in Figure 1b.

Specimens were pulled in tension to a strain of about 5%. They were unloaded, aged at 100C in a boiling water bath for 1 hour and reloaded at the same cross head speed. We could not continuously monitor the crosshead speed in our tests; it was set so that the crosshead moved at 0.02 in/min (0.0085 mm/s) under zero load; this setting was constant throughout a test. (One test was run with a setting of 0.005 in/min (0.0021 mm/s).)

The load and elongation were recorded throughout the test. The separation of gage marks in the reduced section and the specimen diameter were measured before the start of the test and after the initial unloading.

Texture Analysis

Neutron pole figures were taken on six samples from the following dynamic tear specimens:

FZF17, GCM84, GEA20, GEB6, GFF70, GBD364.

The location of the samples is shown schematically in Figure 1c. The first three are from 3/4" plates; the second set of three are from 2 or 2½" plates. Specimens were machined into cylinders having a diameter of 0.5 in and a length of 0.25 in. Complete pole figures were generated by placing the samples in a beam of neutrons having a wavelength of 0.127 nm, selecting the appropriate detector orientation to observe diffraction from crystal planes defined by Miller indices (hkℓ), and measuring beam transmission over a range of sample orientations which span the entire hemisphere above the plane of the plate. Experiments were done at the NBS Reactor and data were converted to pole figures using programs written by C. S. Choi at NBS.

RESULTS

Metallography

Preparing a good metallographic sample in this grade of steel is very difficult. The ferrite is easily cold worked, which makes it appear that there is a substructure in the ferrite or intragranular carbide precipitation. Retention of inclusions through the polishing steps is difficult. The following techniques alleviated some of the problems:[9,10]

1) change the grinding papers frequently; use a paper for only three or four samples;
2) after grinding, polish with 6 μm diamond on a nylon cloth for approximately 1 minute;
3) after polishing on 6μm diamond, go immediately to the final polish with Linde A for approximately 1 minute or go immediately to colloidal SiO_2 for approximately 1 minute.

a) Inclusions

We did not measure inclusion contents in these steels. The difficulties that we encountered in preparing good metallographic samples precluded the use of automatic image analysis. The inclusion contents are uniformly low and the inclusions are generally small, so that measurements are difficult: high magnifications must be used to include the small particles and hundreds of fields would have to have been examined in each specimen to get reasonable statistics.

Every specimen was examined in the as-polished condition and qualitative aspects of inclusion sizes, morphologies and distributions were noted. These are summarized in Table III. Micrographs of some of the inclusions which were found in these steels are shown in Figures 2 through 4. (The micrographs in Figure 2 are taken from earlier work, but they are from plates that are part of the work that is reported here.)

The small inclusions are generally round and appear to consist of more than one phase. In GAG and GES, the small inclusions are angular, reflecting the

lack of calcium additions, which was noted previously.[2] In GAG, stringers of inclusions are also found, Figure 2. Large round inclusions consist of a glassy core and a duller shell, and there may be small particles within the core. A region with a particularly dense array of elongated inclusions is found in GDY10, Figure 3. These are light, dull gray and look like sulfides, although there are occasionally small black particles associated with them. They are not uncommon in any of the plates, although they are difficult to find except in GDY. The similarities in chemistry between GDY and GEB indicate that they are from the same heat, but there was this difference between our two samples.

To examine the elemental make-up of inclusions, we examined the following samples: GEA34, GAG312, GBD364, GEB6, and GDY14. In the two plates in which the inclusion morphologies might be considered typical of the HSLA-80 steels, GBD and GEB, the spectra from EDS analyses show that the inclusions contained Al, Ca, Mn, and S. In Figure 5 are elemental dot maps and the scanning electron microscopy image from two inclusions in GBD. The central dark regions are calcium aluminates and these are surrounded by (Ca,Mn)S shells.

In GAG, the elongated inclusions are MnS and the smaller, equiaxed ones are mostly aluminates. In GDY, the elongated inclusions are again MnS. A dot map of a typical sulfide from GDY is given in Figure 6. The round inclusions in that plate are complex; the elemental dot maps and SEM image for a typical 10μm diameter particle are shown in Figure 7. It shows that the calcium aluminate core is surrounded by (Ca,Mn)S, similar to that in Figure 5.

The large inclusions which are typical of GEA contained Mg, Al, Si, Ca, Mn, Fe, and S. Dot maps and the SEM image from a 15 μm inclusion are shown in Figure 8.

b) Microstructure

Micrographs of the center regions of the metallographic samples are shown in Figure 9 through 13. Grain sizes were not measured in any of these samples. The microstructures are non-polygonal in several of them and grain size is not well-defined in such a structure. There were often variations in structure through the thickness, as well. In samples in which it was possible, grain sizes were estimated. These are listed in Table IV.

One aspect of the non-uniformity in structure is microstructural banding. Examples are shown in Figure 14 through 16. This banding is most likely the result of carbon and manganese segregation from ingot solidification. These elements increase the hardenability so that low-temperature transformation products form in those regions. Further evidence that this is the case is that elongated sulfides, which are MnS, are concentrated in the "bainite streaks". Examples of this are shown in Figure 17.

Two of the samples, GEB6 and GBD364, were repolished and lightly etched in picral and HCl, to allow examination of carbide morphologies using the SEM. Scanning electron micrographs are shown in Figures 18 and 19.

Strain Aging Tests

The simplest measure of the amount of strain aging is usually taken to be the

strain aging index. This is the difference between the flow stress at unloading, prior to aging, and the yield stress at reloading, after aging. The stress-strain curve from GEA20, which exhibits the largest strain aging index of the three plates examined is shown in Figure 20. The index is indicated schematically. A summary of the results of these tests is given in Table V.

Texture Analyses

a) Theory

In this report we utilize the notation and methods developed by Roe[11] and Allen[12]. We begin by defining an orientation distribution function (ODF), $w(\xi,\psi,\phi)$. Angles ξ, ψ, and ϕ are Euler angles which relate grain orientation with respect to bulk sample axes. In the case of steel plates, crystallographic axes are defined along the three cube directions of the iron unit cell and the sample axes are defined along the rolling, normal and transverse directions of the plate. The function $w(\xi, \psi, \phi)$ gives the number of grains whose orientation is within $\Delta\xi$, $\Delta\psi$, and $\Delta\phi$ of the specified Euler angles.

The orientation distribution function can be expanded in terms of generalized spherical harmonics, as given by Roe [11]:

$$w(\xi, \psi, \phi) = \sum_{\ell=o}^{\infty} \sum_{m=-\ell}^{\ell} \sum_{n=-\ell}^{\ell} W_{\ell mn} Z_{\ell mn}(\cos \xi)\, e^{-im\psi} e^{-in\phi} \qquad (1)$$

where the $W_{\ell mn}$'s are orientation distribution function coefficients (ODC's), which quantitatively describe the crystallographic texture of a sample, and $Z_{\ell mn}(\cos \xi)$ is a generalization of the associated Legendre function, P_{ℓ}^{m}. Values of the ODC's are determined by measuring pole figures, $q_i(\zeta, \eta)$ and fitting the data to an expansion in spherical harmonics:

$$q_i(\zeta, \eta) = \sum_{\ell=o}^{\infty} \sum_{m=-\ell}^{\ell} Q_{\ell m}^{(i)} P_{\ell}^{m}(\cos \zeta) e^{-im\eta} \qquad (2)$$

Here the subscript $\underline{i}$ denotes a choice of Miller indices corresponding to a particular diffraction condition. The polar and azimuthal angles ζ and η describe the orientation of the sample (i.e. the plate normal) with respect to the scattering vector.

The $Q_{\ell m}$'s obtained from a fit to the measured pole figure could be used to determine the orientation distribution function coefficients ($W_{\ell mn}$'s) through the following relation:

$$Q_{\ell m}^{(i)} = (2\pi) \left\{ \frac{2}{2\ell + 1} \right\}^{1/2} \sum_{n=-\ell}^{\ell} W_{\ell mn}\, P_{\ell}^{n}(\cos \Theta) e^{in\Phi} \qquad (3)$$

Angles Θ and Φ are polar and azimuthal angles describing the orientation of the reciprocal lattice vector $(hk\ell)$ with respect to the unit cell crystallographic axes. For our purposes, however, it is sufficient to extract

the values of Q from our data and use these to establish a relative measure of texture with which to compare samples.

Quantitative analysis of the pole figure data was accomplished with a program which inverts equation 2 and uses measured pole figure data to compute the $Q_{\ell m}$'s up to a maximum of ℓ=10. The choice of maximum ℓ was dictated by computational considerations and the fact that higher values of ℓ represent small deviations from the overall texture of the plate. Since in this study, we were interested in developing a relative measure of texture, only values corresponding to ℓ=4 and ℓ=6 will be reported.

b) Results

Pole figures determined from the six samples are given in Figures 21 and 22.

The spatial dependence of the pole figures shows that there are several crystal orientations that are favored when the plates are deformed by rolling: <110> directions tend to cluster around the rolling direction and <111> directions seem to favor the plate normal.

Figure 23 shows $Q_{\ell m}$'s for ℓ=4 and ℓ=6 for the (110) pole figures for the 3/4 inch plate specimens. Note that values of Q_{4m} are close to zero for all three plates, whereas values of Q for ℓ=6 are clearly nonzero and show a significant difference from plate to plate. Since larger values of Q denote stronger texture, we can see from the data in Figure 23 that FZF17 is much more stongly textured than GEA20 and GCM84. The data also distinguishes between GEA20 and CGM84: GCM84 has the smallest amount of crystalline texture in the 3/4 inch plates studied. This can be seen qualitatively in a comparison of the 3/4 inch plate pole figures shown in Figure 21.

As might be expected, the texture observed in 2 and 2½ inch plates is much weaker than that in the 3/4 inch plates, Figure 24. In addition, the values of all $Q_{\ell m}$'s in the thick plates were found to vary with depth in the plate. This is shown in Figure 25, in which pole figures from opposite faces of the dynamic tear specimen GEB6 are shown. The sample with the stronger texture is assumed to come from the part of the dynamic tear specimen that was closer to the plate center.

DISCUSSION

In this discussion, we attempt to relate the chemistries and microstructures of these steels to their mechanical behavior. The relationships must remain qualitative because of the difficulties we had in making measurements. Furthermore, we have not considered some of the more important strengthening agents in A710 grade steels, such as copper and columbium carbo-nitride precipitates.

Of special concern is the relationship between the microstructure and chemistry and the behavior in the explosion bulge test. These plates were not tested under the usual conditions with two sections of plate welded together

as the test sample. Instead, a starter bead was applied to a section of plate which was then tested.

Inclusion contents depend upon the sulfur concentrations.[13] All of these steels have less than 0.008w/o S, so the inclusion contents are low. Toughness and ductility are the mechanical properties that are most strongly affected by inclusions. Since the sulfur contents are uniformly low, variation in the toughness and ductility that are due solely to differences in the amounts of sulfur are probably small.

In a few of the plates, GCM, GEA, GDY, and GEB, we find large, globular inclusions; examples are shown in figures 3 and 8. Two others plates, GAG and GES, did not contain calcium and had no sulfide shape control.

The globular inclusions cannot be clearly implicated as detrimental in these steels. Plates GEA and GEB do not meet the toughness requirements of MIL-S-24645 at -120F: the lowest values of absorbed energy at that temperature are below 30 ft-lbs. However, the impact properties of GCM and GDY are within specifications. The inclusion morphology may be responsible for the low toughness in GEA, since they were particularly large in that plate. The comparatively poor toughness of GEB, which is from the same heat as GDY, is likely due to its very high strength.

In the past, large, globular inclusions have been a particular problem with calcium-treated steels; they result from poor steel making practices.[14] The Mg in inclusions in GEA probably comes from furnace or ladle refractories or from the slag. In either case, its presence within the product is not desirable. There have been advances in ladle metallurgy and, in particular, in calcium treatment in the past few years.[15-17] These types of inclusions should not be present, even though they may not be the clear cause of problems here.

The two plates without shape control have lower absorbed energies at room temperature and 0F than other plates of the same thicknesses. Neither GAG nor GES meets the impact requirements at -120F. A major effect of sulfide shape control is to increase the upper shelf energy.[18,19] The lower toughness of these two plates at the higher test temperatures is in line with that. Sulfide shape control can be more effective in improving toughness and ductility than further reductions in sulfur content in steels that are low in sulfur to begin with.[19]

The three that passed explosion bulge tests, FZF, GES, and GBD, all had low inclusions contents, but so did plates that failed. Lack of shape control in GES appears not to be a problem. Plate GEA, with large, globular inclusions, is rated as a marginal failure in that test. Thus, inclusion content and morphology cannot be related to a plate's behavior in the explosion bulge test.

We usually take strength to be determined by ferrite grain size, solid solution hardening and precipitation strengthening. For ferrite-pearlite steels, the quantitative relationships have been well developed. For non-polygonal ferrite or bainitic steels, that is not the case.[20,21] In A710

grade steels, the carbide content and distribution might also play a role, as do the martensite-austenite islands in dual phase steels, but we are not aware of studies concerned with it. Comparisons of microstructures in figures 9 through 13 show that a range of grain sizes and different ferrite morphologies can give essentially the same strength levels in these steels. However, there are not any good means for us to describe how these variations alone affect the strength because Cu and Cb(C,N) precipitates are important determinants of strength in these steels, and we did not look at them.

The plates with the best toughness at each thickness are FZF (3/4 in), GDY (1 in), FUQ and the re-heat treated section of GBC (1¼ in), and GFF (2 in). The 2½ in plate, GBD, also has good toughness. (We do not know which of our samples from GBC had been heat treated twice, so we cannot consider it further.) With the exception of GDY, these plates have polygonal ferrite microstructures. Other investigators have found that better toughness in steels with this chemistry is associated with polygonal ferrite.[22-24]

The non-polygonal microstructures in these steels are likely due to coarser parent austenite grains. They might be due to faster cooling rates from austenitization in the thinner gages or to richer chemistries. Neither of these explanations for the increased "hardenability" seems satisfactory, however. The chemistry variations are not wide enough and GEA and GCM simply appear to have coarser microstructures than GZF and GAG. Even though we cannot detect prior austenite grain boundaries, it is reasonable to expect that the plates with non-polygonal microstructures, a low-temperature transformation product, had coarser grain sizes at austenitization than those with polygonal microstructures.

In bainitic steels, the toughness is reduced when the parent austenite grain size is coarser.[21] The high angle boundaries, which are the bainite "packet" boundaries, determine the impact behavior. The same effect could be working in these steels; in polygonal ferrite, the high angle boundaries are the ferrite grain boundaries; in acicular microstructures, they are the prior austenite boundaries. The finer "effective" grain size in the former gives better toughness.

The behavior in the explosion bulge tests is not unambiguously related to ferrite morphology, but a polygonal microstructure might be advantageous. Two of the plates that passed, FZF and GBD, are polygonal ferrite, and GES contains some. And plate GFF, which marginally failed, has a fine-grained ferritic microstructure. However, plates FUQ and GGN, both with fine-grained, polygonal microstructures, failed the test.

Crystallographic texture may also play a role in determining explosion bulge behavior. Our data are not sufficient, however, to make a firm case. Among the 3/4 in plates, the best combination of properties is in FZF, which has the strongest texture among the plates examined. The {111}<110> texture, for which we find some tendencies, gives significant strengthening under biaxial loading.[8] It also has the {100} cleavage planes off of the principal directions of the plate and so may toughen it.[25] However, in plates, the texture varies from random at the surface to "maximum" in the center[26,27], which is in line with our finding on the thicker plates. It is difficult to

analyze how texture might affect properties, although it appears to play a role in splitting in controlled-rolled plates.[25]

It is also not easy to understand why there should be any texture in these plates at all. In hot-rolled plates, the recrystallization that occurs during processing is expected to eliminate most of the crystallographic alignment of the deformed austenite. Furthermore, the austenitization will also reduce texture. Without some better understanding of why there is any texture in some of these plates, it is probably not reasonable to suggest that it has an effect on properties. It would also be valuable to examine the variation through the entire thickness of a plate.

The one variable that clearly distinguishes between plates that passed the explosion bulge test and those that failed is the ratio of aluminum to nitrogen in the steel. This is shown in Figure 26, in which each plate is a point determined by Al/N and N-content, with behavior in the explosion bulge test indicated. Values are tabulated in Table VI. The nitrogen content is not so clear in its ability to discriminate between the two types of behavior, but the three plates that passed the test have low to moderate nitrogen contents, and rarely can the effect of Al/N be considered without taking the total nitrogen content into consideration as well.

The aluminum-to-nitrogen ratio can be expected to influence the mechanical properties either through grain-size control during slab reheat, hot rolling and austenitization or by influencing the amount of interstitial nitrogen in solid solution. The strain aging tests can give a measure of the amount of free nitrogen when it is low.[29] We estimate that in GEA it is about 0.0005 w/o, which is a very small amount. In the other two plates, it is less. This is not unexpected because nitrogen in these steels can be tied up by Cb and Cr, as well as Al.

However, the negative results of our strain aging tests do not eliminate the possibility that strain aging or embrittlement due to mobile nitrogen causes failure in the explosion bulge tests. Applying the starter bead to the plate creates a heat affected zone in which some of the nitrides can dissolve. Nitrogen can also be picked up from the atmosphere. Reprecipitation of nitrides may not occur readily. For stoichiometric CbN, Cb/N should be 6.6, which is approached in some of the plates, but Cb is more likely to form a carbide; CrN precipitation occurs at low temperatures and so is very sluggish. For AlN precipitation to occur and remove a significant amount of interstitial nitrogen, there should be more than the stoichiometric amount, Al/N = 1.96. In the heat affected zones around the starter beads on many of these plates, it is likely that there are significant amounts of mobile nitrogen.

There is a better test to determine whether mobile nitrogen is indeed the cause of explosion bulge failures. Tensile bars could be subjected to a thermal cycle to simulate that of the HAZ, using a Gleeble or similar set-up. Strain aging tests could then be performed on these treated bars.

Another effect of low Al/N ratios can be to allow grain growth during slab reheating and hot rolling. At high temperatures, the austenitic grain boundaries are pinned by small AlN precipitates; Cb(C,N) precipitates can do

the same. If the Al content is low, then the solution temperature for AlN is low, and there may not be enough precipitates available for inhibiting grain growth. We have noted above that some of the plates have non-polygonal microstructures and that these are evidence of coarser, parent austenite grain sizes. Among the steels that have mostly polygonal ferrite microstructures, Table IV, only FUQ has a low Al/N ratio. Plates GGN and GBC have marginal values as far as success in the explosion bulge test is concerned. Those two plates may contain enough Al for austenite grain refinement, to give a polygonal ferrite microstructure, but not enough to tie up the mobile nitrogen in the starter bead's HAZ.

CONCLUSIONS AND RECOMMENDATIONS

All of the plates examined in this work have low inclusion contents, because of effective desulfurization. However, in some cases, we find large, globular inclusions, which indicate poor steelmaking practices. These are not clearly associated with poor performance in the mechanical tests for this grade, but should not be tolerated. Sulfide shape control is necessary for excellent high-temperature toughness.

The microstructures in these plates can consist of fine-grained, polygonal ferrite with islands of higher-carbon transformation products, which are tempered martensite and, probably, bainite. It can also be a non-polygonal ferrite; the carbide distributions are more difficult to describe for those structures, but appear to be islands as well as discrete particles. The best combinations of strength and toughness are found in steels with polygonal microstructures. Crystallographic texture may also be related, but our data are insufficient to explain how it varies from plate to plate and how it might affect properties.

The three plates that were tested for strain aging due to free nitrogen exhibited only a small amount. This does not eliminate the possibility that this mechanism is responsible for failure in explosion bulge tests. Nitrogen that is combined in nitride precipitates in the plate can be put into solution in the heat affected zone of the weld or starter bead in explosion bulge specimens. Further tests are required.

That mobile nitrogen may be responsible for bulge test failures is made more likely by the observation that plates with high Al/N ratios pass the test. When the ratio is high, more nitride precipitation occurs, because the driving force is higher and kinetics are faster. Consideration should be given to specifying lower nitrogen contents and an appropriate range for aluminum. Further study and discussions with steelmakers are necessary to determine what those limits should be.

REFERENCES

1. E.J. Czyryca, DTNSRDC Private Communication, June 1986.

2. Mary Jean Crooks and George E. Hicho, Memorandum to Ernest J. Czyryca, "Chemical Compositions of HSLA 80 Plates, September 15, 1986.

3. G.E. Hicho, NBS, Private Communication, September 15,1986.

4. L.A. Erasmus and L.N. Pussegoda, "The Strain Aging Characteristics of Reinforcing Steel with a Range of Vanadium Contents," Met. Trans. 11A (1980) 231.

5. T. Gladman, "On the Theory of the effect of precipitate particles on grain growth in metals," Proc. Royal Soc. 294A (1966) 298.

6. K.J. Irvine, F.B. Pickering, and T. Gladman, "Grain-refined C-Mn steels," JISI 205 (1967) 161.

7. G.R. Speich and T. Scoonover, DTNSRDC Unpublished Research.

8. W.A. Backofen, Deformation Processing, (Reading, Mass: Addison-Wesley Publishing Company, c. 1972), Chapters 3 and 4.

9. C.H. Brady, NBS, Private Communication, January 20, 1987.

10. A.O. Benscoter, Bethlehem Steel Corp., Private Communication, July 1986.

11. R-J Roe, J. Appl. Phys. 37 (1966) 2069.

12. A.J. Allen, M.T. Hutchings, C.M. Sayers, D.R. Allen and R.L. Smith, J. Appl. Phys. 54 (1983) 555.

13. G.F. Van der Voort, "Inclusion Measurement," Metallography As a Quality Control Tool (New York: Plenum Publishing Corporation, c. 1980) 1.

14. G.F. Van der Voort, Carpenter Technology Corp., Unpublished Research at Bethlehem Steel Corp.

15. Scaninject III, Refining of Iron and Steel by Powder Injection, (Lulea, Sweden: MEFOS, 1983).

16. Scaninject IV, ed. by G. Carlson (Lulea, Sweden: MEFOS, 1986).

17. Steelmaking Conference, Proceedings (Warrendale, PA: ISS-AIME, 1983).

18. J.L. Mihelich, J.R. Bell and M. Korchynsky, "Effect of Inclusion shape on the Ductility of Ferritic Steels," JISI 209 (1971) 469.

19. W.A. Spitzig and R.J. Sober, "Influence of Sulfide Inclusions and Pealite Content on the Mechanical Properties of Hot-Rolled Carbon Steels," Met. Trans 12A (1981) 281.

20. F.B. Pickering, "The Optimisation of Microstructures in Steel and Their Relationship to Mechanical Properties," Hardenability Concepts with Applications to Steel, ed. by D.V. Doane and J.S. Kirkaldy (Warrendale, PA: TMS-AIME, c. 1978) 179.

21. Terry Gladman, David Dulieu, and Ian D. Mclvor, "Structure-Property Relationships in Microalloyed Steels," MicroAlloying 75 (Danbury, CT: Union Carbide Corp., c. 1977) 32.

22. Edwin Snape, "The Effects of Experimental Rolling on Microstructure and Mechanical Properties of a Ni-Cu-Cb Steel," Met. Trans 1 (1970) 1375.

23. P.P. Hydrean, A.L. Kitchin, and F.W. Schaller, "Hot Rolling and Heat Treatment of Ni-Cu-Cb(Nb) Steel," Met. Trans 2 (1971) 2541.

24. M.T. Miglin, J.P. Hirth, and A.R. Rosenfield, "Effects of Microstructure on Fracture Toughness of a High-Strength Low-Alloy Steel," Met. Trans 14A (1983) 2055.

25. B.L. Bramfitt and A.R. Marder, "Splitting Behavior in Plate Steels," Toughness Characterization and Specifications for HSLA and Structural Steels ed. by P.L. Mangonon, Jr. (Warrendale, PA: TMS-AIME, c. 1979) 236.

26. G.R. Speich and D.S. Dabkowski, "Effect of Deformation in the Austenite and Austenite-Ferrite Regions on the Strength and Fracture Behavior of C, C-Mn, C-Mn-Cb, and C-Mn-Mo-Cb Steels," The Hot Deformation of Austenite, ed. by John B. Ballance (New York: TMS-AIME, c. 1977) 557.

27. G.J. Davies, J.S. Kallend, and P.P. Morris, "The Influence of Hot Deformation of Austenite on the Properties of Ferrite Through the Development and Inheritance of Texture," The Hot Deformation of Austenite, ed. by John b. Ballance (New York: TMS-AIME, c. 1977) 599.

28. B. Mintz, "Influence of cooling rate from normalizing temperature and tempering on strength of ferrite-pearlite steels,", Met. Tech. 11 (1984) 52.

TABLE I. SELECTED MECHANICAL PROPERTIES OF HSLA-80 PLATES

Sample Code	Plate Thickness in	Yield Strength ksi	Tensile Stength ksi	Elong. %	Red. of Area %	CVN Impact Tougness + RT ft-lbs	CVN Impact Tougness + -120F ft-lbs	Explosion ++ Bulge
FZF17	3/4	91.3	104.3	28	73	170	131	Pass
FZF30						152	101	3 - 20%
GAG300	3/4	87.2	101.5	27	70	150	66	No test
GAG312						130	29	
GCM84	3/4	90.7	102.7	35	76	174	56	Fail
						168	42	3 - 10%
GEA20	3/4	86.4	99.0	36	74	151	61	Fail (marg
GEA34						138	8	3 - 14%
GDY10	1	92.0	104.5	35	69	147*	88	Fail
GDY14						126*	46	3 - 7%
GES15	1	94.0	106.7	28	73	123	35	Pass
GES26						116	29	4 - 16%
FUQ105	1-1/4	82.8	97.9	30	77	186	110	Fail
						174	104	3 - 6%
GBC33**	1-1/4							
GBC30**								
GBCH1**								
GEB6	2	87.0	105.1	36	71	80*	7	Fail
GEB14						64*	4	1 - 0%
GFF66	2	74.2	87.0	32	80	240	206	Fail (marg
GFF70						240	150	3 - 14%
GGN4	2	Not available						Fail
GGN48								
GBD12	2-1/2	77.3	90.5	30	76	178*	84	Pass
GBD364						168*	70	4 - 16%

+ The values of absorbed energy are the highest and lowest at these temperatures.
++Explosion Bulge Test results are Pass, Fail and Marginal Fail
First number is number of shots; second number is percent reduction in thicknes
* Measured at 0F
** This plate failed the explosion bulge test, was re-heat-treated and then passed. not sure of the individual histories of these samples.

TABLE II. CHEMISTRIES OF HSLA-80 STEELS

Plate	C	Mn	P	S	Si	Ni	Cr	Mo	Cu	Sn	V	Ti	Nb	Al	Ca	N
FZF*	.054	.546	.0047	.0047	.265	.915	.739	.208	1.24	.011	.003	.003	.0508	.0498	.0039	.00846
GAG*	.038	.520	.0021	.0078	.316	.927	.684	.199	1.18	.012	.002	.002	.0413	.0419	.0003	.00749
GCM	.043	.674	.0043	.0034	.203	.909	.824	.189	1.18	.009	.004	.002	.0389	.0177	.0024	.00829
GEA*	.040	.633	.0060	.0061	.342	.889	.724	.185	1.18	.010	.003	.003	.0397	.0269	.0048	.01406
GDY*	.050	.675	.0070	.0075	.360	.935	.744	.197	1.27	.010	.004	.003	.0494	.0221	.0024	.01513
GES*	.045	.666	.0128	.0048	.328	.912	.753	.180	1.10	.003	.005	.003	.0446	.0572	.0006	.00401
FUQ	.044	.615	.0058	.0028	.290	.900	.681	.196	1.25	.008	.003	.002	.0498	.0233	.0037	.01285
GBC**	.039	.637	.0051	.0037	.273	.791	.866	.216	1.20	.009	.003	.004	.0470	.0311	.0019	.00822
GEB*	.048	.665	.0072	.0075	.355	.932	.742	.194	1.25	.011	.004	.003	.0474	.0225	.0028	.01487
GFF*	.040	.586	.0052	.0043	.246	.900	.701	.188	1.17	.006	.003	.002	.0333	.0412	.0023	.01458
GGN*	.058	.536	.0063	.0014	.269	.913	.759	.219	1.26	.014	.005	.004	.0476	.0365	.0022	.00990
GBD*	.036	.633	.0044	.0036	.269	.782	.865	.215	1.18	.008	.003	.004	.0467	.0307	.0020	.00777

*Averages from two dynamic tear specimens

** Averages from three dynamic tear specimens

All steels except GGN contained residual amounts of B (<0.0004 w/o); GGN contained 0.0008 w/o B

All steels contained <0.008 w/o Ta, <0.001 w/o Zr, <0.007 w/o As

TABLE III. INCLUSIONS IN HSLA-80 PLATES

Code	Plate Thickness	
FZF	3/4	Low inclusion content. Some oxide stringers. Inclusions are generally very small, but there are some 10μm.
GAG	3/4	Low inclusion content. No shape control; inclusions are not round. They are all less than 10μm.
GCM	3/4	There are many large, round inclusions, around 50 μm. There are some elongated inclusions.
GEA	3/4	There are many large, globular inclusions, greater than 50 μm. This is the worst plate of the set.
GDY	1	Low inclusion content. A common feature is elongated sulfides. Round inclusions are usually less than 10μm; there are occassional large inclusions.
GES	1	Low inclusion content. Very small inclusions are angular, not rounded.
FUQ	1-1/4	Low inclusion content.
GBC	1-1/4	Low inclusion content.
GEB	2	There are many small inclusions, 5 to 10μm and some large ones, 50μm. They are all complex (multiphase) and rounded.
GFF	2	Low inclusion content. Inclusions are often clustered in colonies which contain rounded inclusions 5 to 20 μm.
GGN	2	Low inclusion content. Most inclusions are small and rounded. There are some elongated ones.
GBD	2-1/2	Low inclusion content. Most inclusions are rounded and less than 10 μm.

TABLE IV. ESTIMATED ASTM GRAIN SIZE NUMBER IN SOME HSLA80 PLATES

Code	Plate Thickness	ASTM Grain Size Number
FZF17	3/4	12 to 12.5
FZF30		11.5 to 12
FUQ105	1¼	11.5 to 12
GBCH1	1¼	10 to 10.5
GFF66	2	11 to 11.5
GFF70		10.5 to 11
GGN43	2	9 to 9.5
GBD364	2½	9.5 to 10
GBD712		9.5 to 10

TABLE V. STRAIN-AGING TEST RESULTS

Sample	Strain at unloading	Stress (ksi)	Stress at reloading (ksi)	Strain-Aging Index (ksi)
FZF17A*	.064	103480	105000	1.5
FZF17B	.054	102700	103900	1.2
GCM84A	.053	102600	104000	1.4
GCM84B	.045	99580	101260	1.7
GEA20A	.054	97650	99680	2.0
GEA20B	.054	97290	99680	2.4

TABLE VI. Al/N RATIOS IN HSLA-80 PLATES

Plate	Al	N	Al/N	Explosion Bulge Test
FZF	.050	.0085	5.9	Pass
GAG	.042	.0075	5.7	NO TEST
GCM	.018	.0083	2.2	Fail
GEA	.027	.0141	1.9	Fail (marginal)
GDY	.022	.0151	1.5	Fail
GES	.057	.0040	14.2	Pass
FUQ	.023	.0129	1.8	Fail
GBC	.031	.0082	3.8	
GEB	.023	.0149	1.5	Fail
GFF	.041	.0146	2.8	Fail (marginal)
GGN	.037	.0099	3.7	Fail
GBD	.031	.0077	4.0	Pass

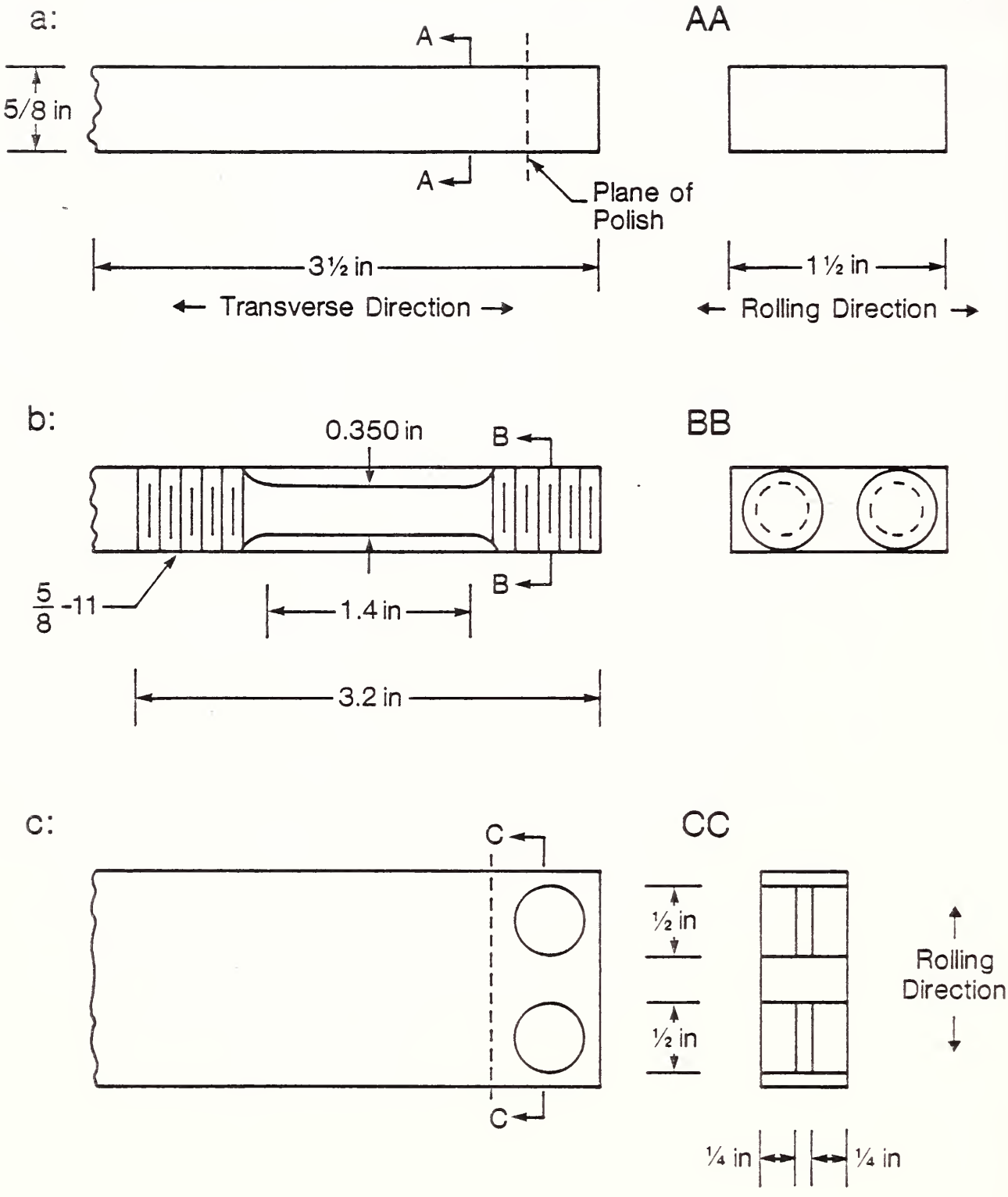

Figure 1. Schematic illustrations of locations and orientations of specimens cut from dynamic tear specimens. a) Metallography, b) Strain-Aging Tests, and c) Pole-Figure Determinations.

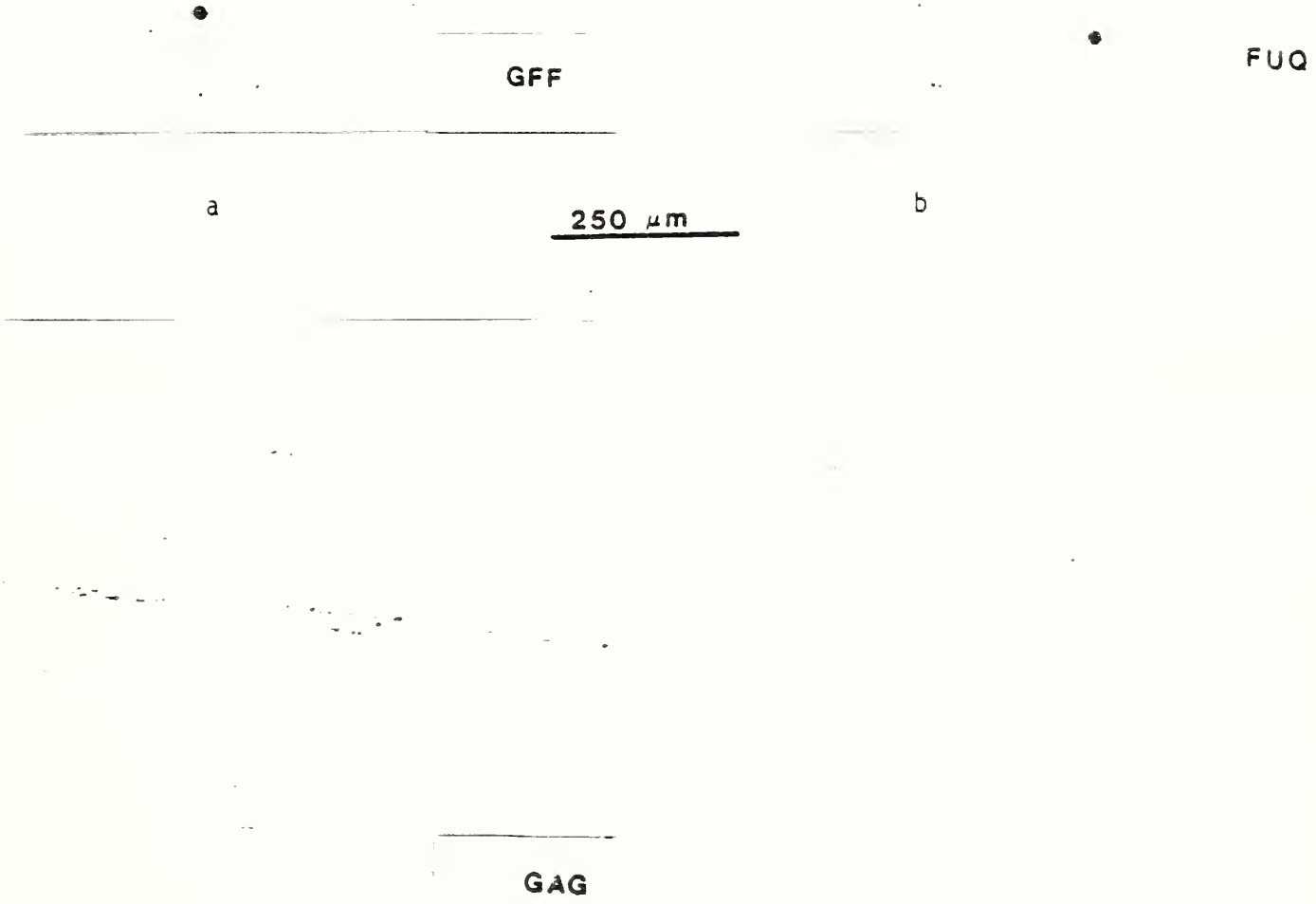

Figure 2. Micrographs of as-polished surfaces in a) GFF, b) FUQ, and c) GAG. Magnification is 100X.

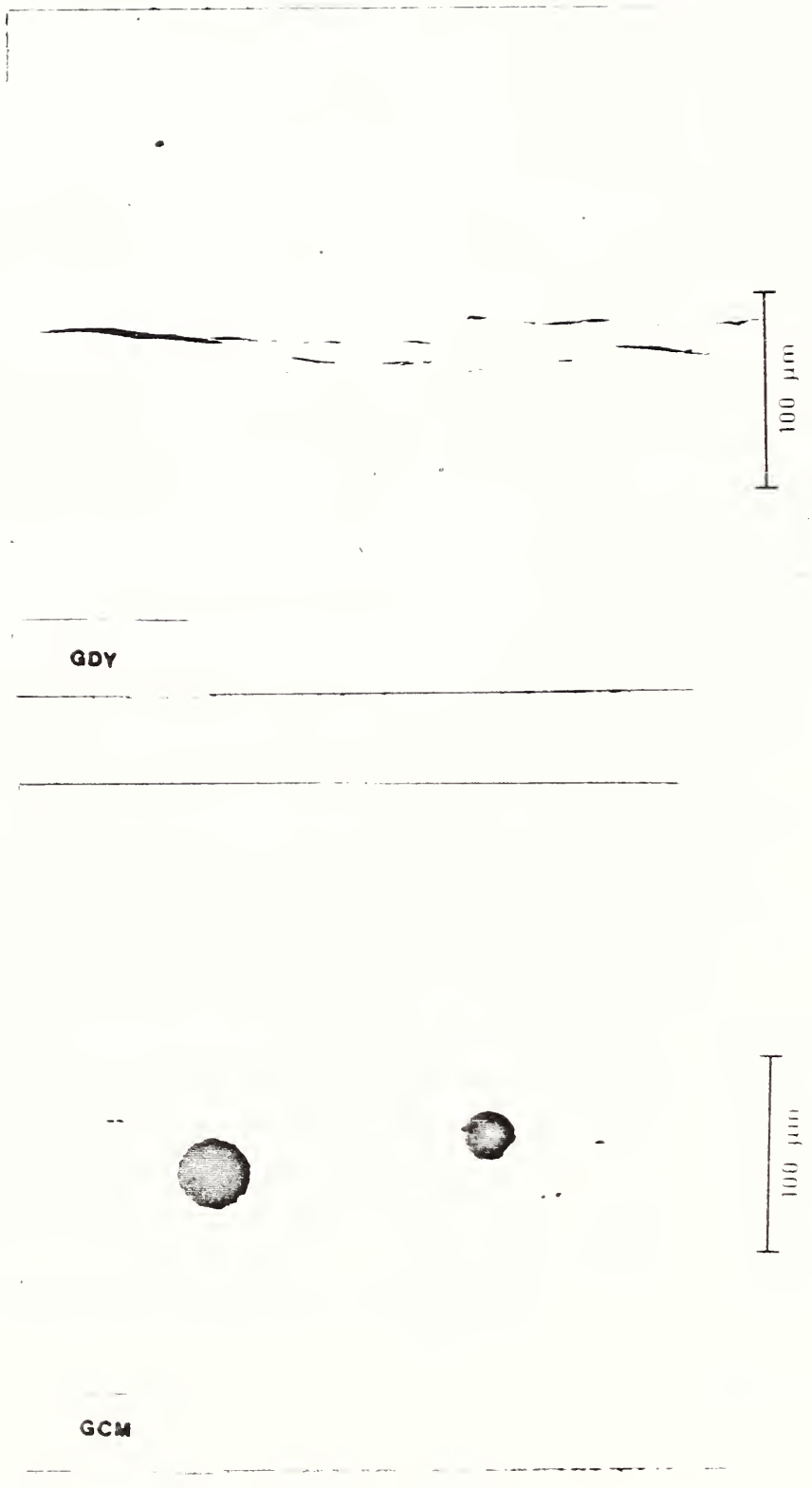

Figure 3. Micrographs of as-polished surfaces showing unusual inclusions in GDY (top) and GCM (bottom). Magnification is 250X.

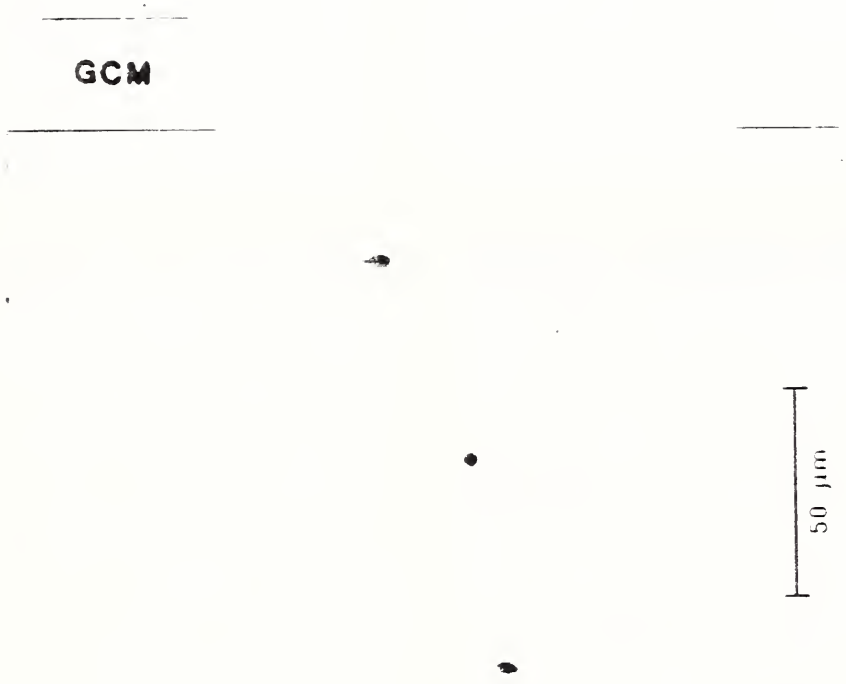

Figure 4. Micrograph of as-polished surface in GCM showing small typical inclusions. Magnification is 500X.

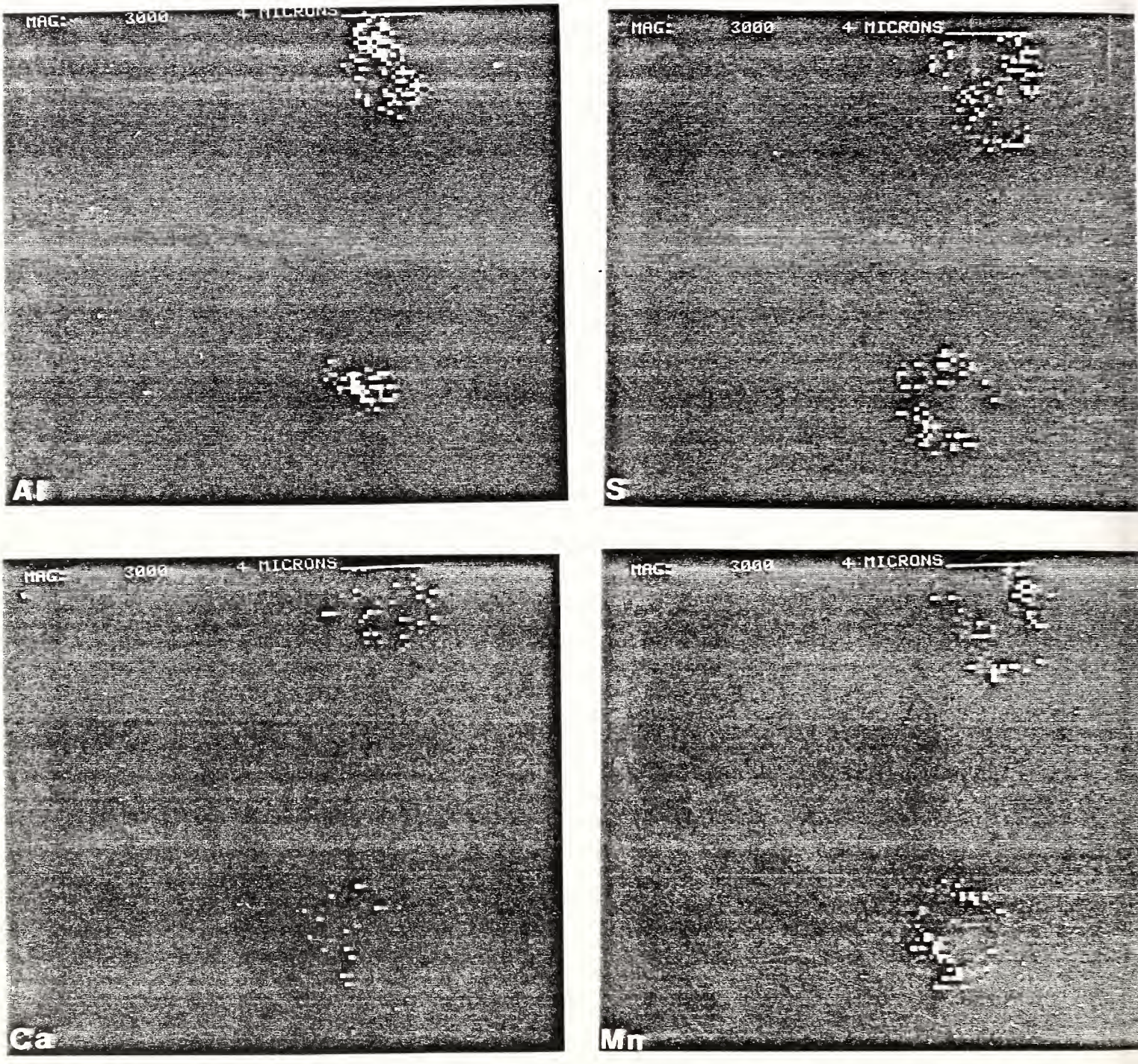

Figure 5. Elemental x-ray dot-maps for Al, S, Ca and Mn and SEM image for inclusions in GBD. Magnification is 3000X.

Figure 5 cont.

SEM

GBD

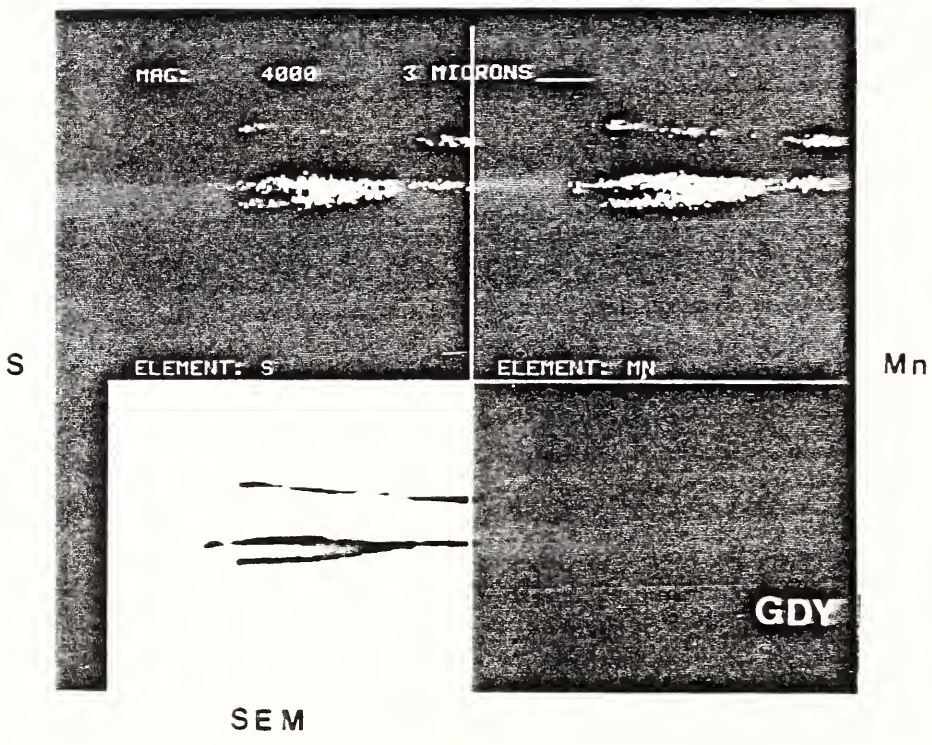

Figure 6. Elemental x-ray dot maps for Mn and S and the SEM image for a sulfide inclusion in GDY. Magnification is 2000X.

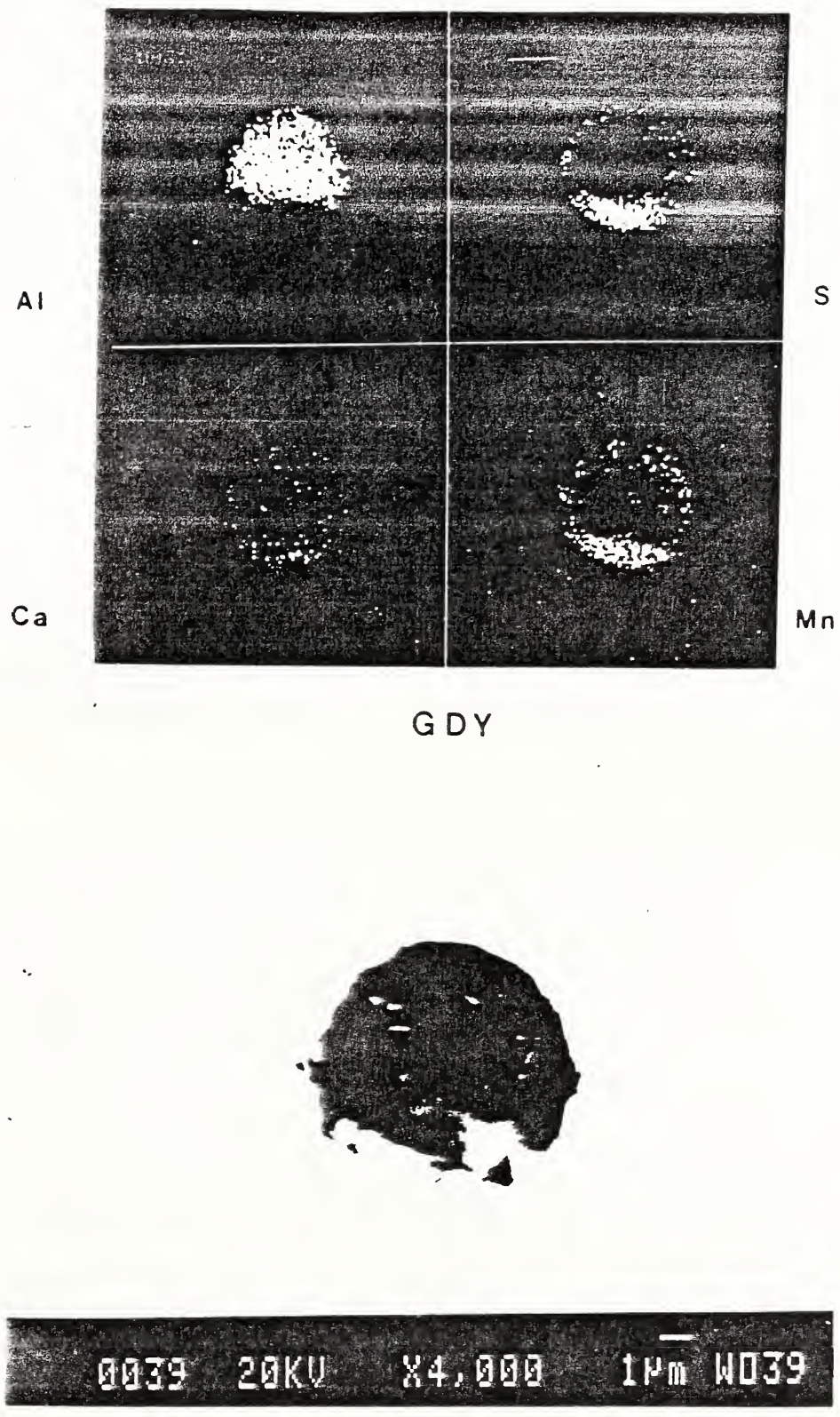

Figure 7. Elemental x-ray dot maps for Al, S, Ca and Mn (magnification, 2000X) and SEM image (magnification, 4000X) for an inclusion in GDY.

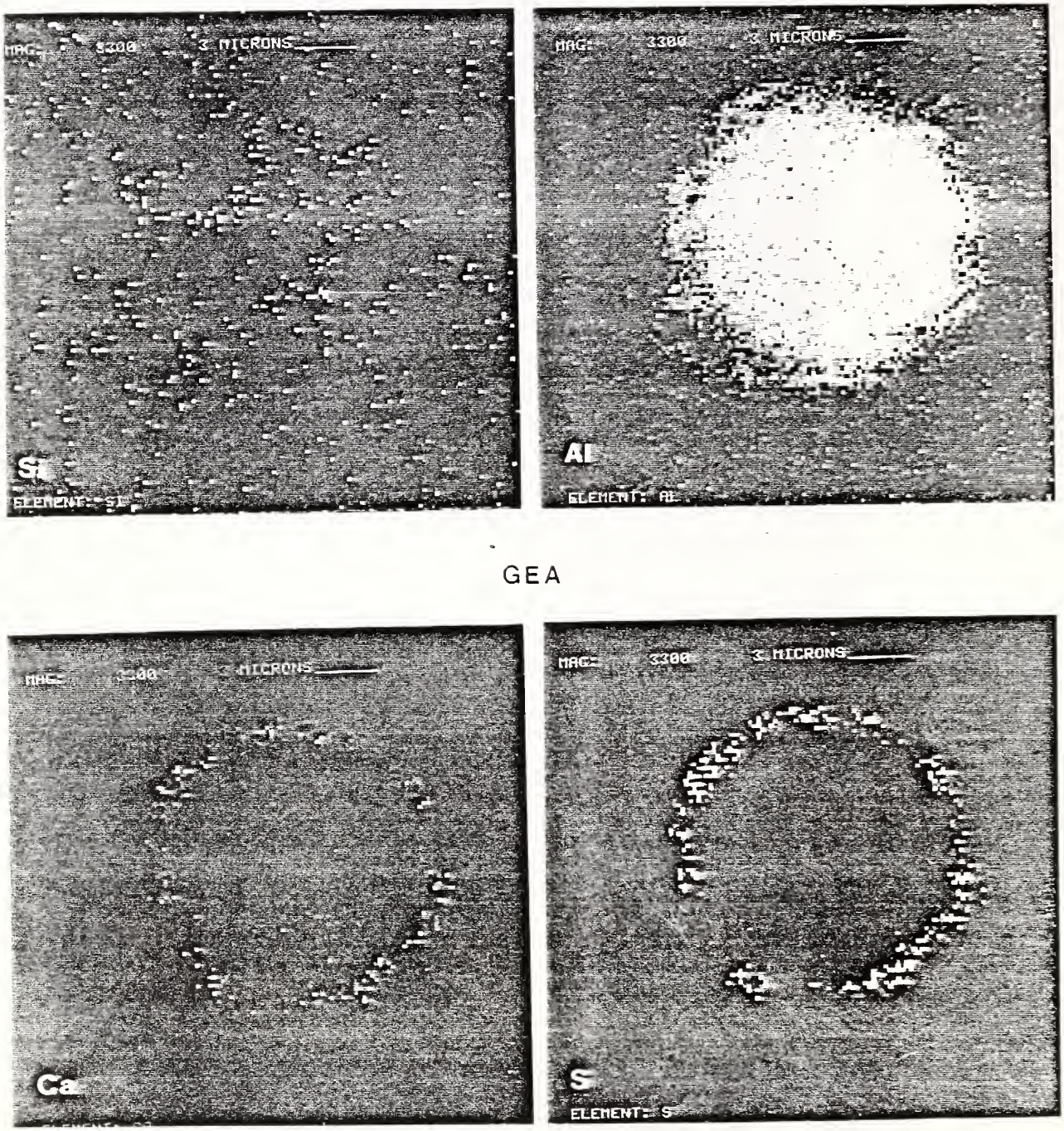

Figure 8. Elemental X-ray dot maps for Si, Al, Ca, S, Mg, and Mn and the SEM image for a large inclusion in GEA. Magnfication is 3300X.

Figure 8 cont.

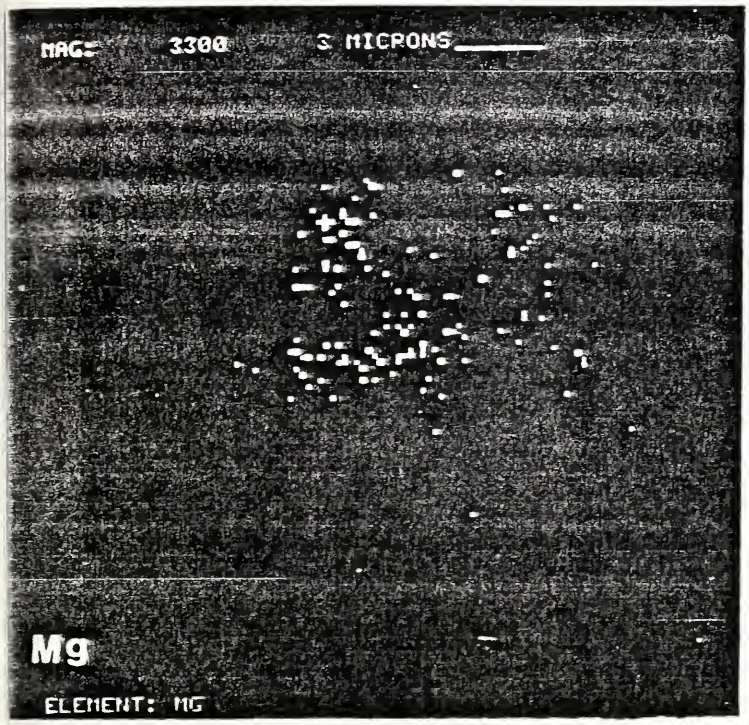

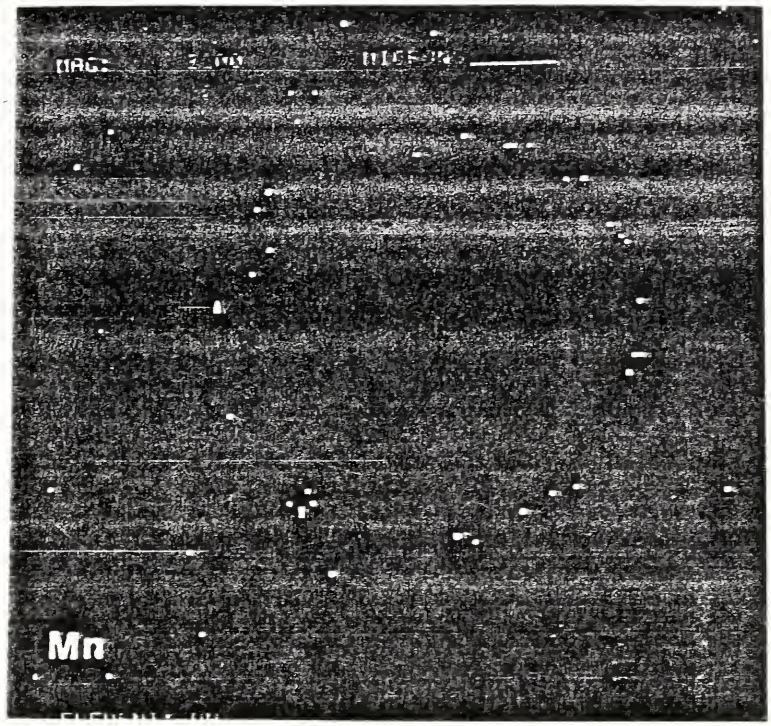

GEA

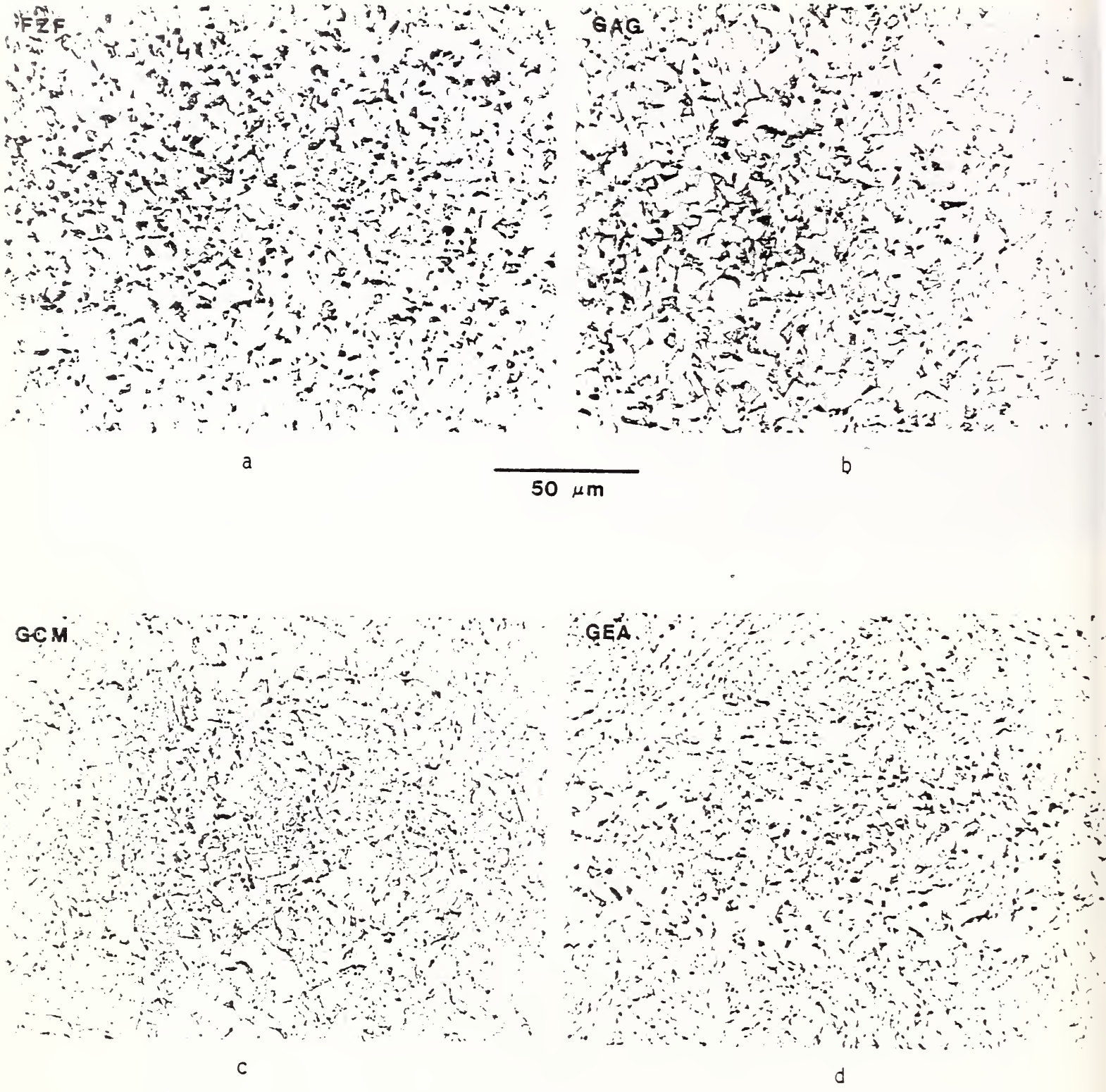

Figure 9. Light micrographs of samples from 3/4 in plates: a) FZF, b) GAG, c) GCM, and d) GEA. All samples were etched in 2% nital; magnification is 500X; rolling direction is horizontal.

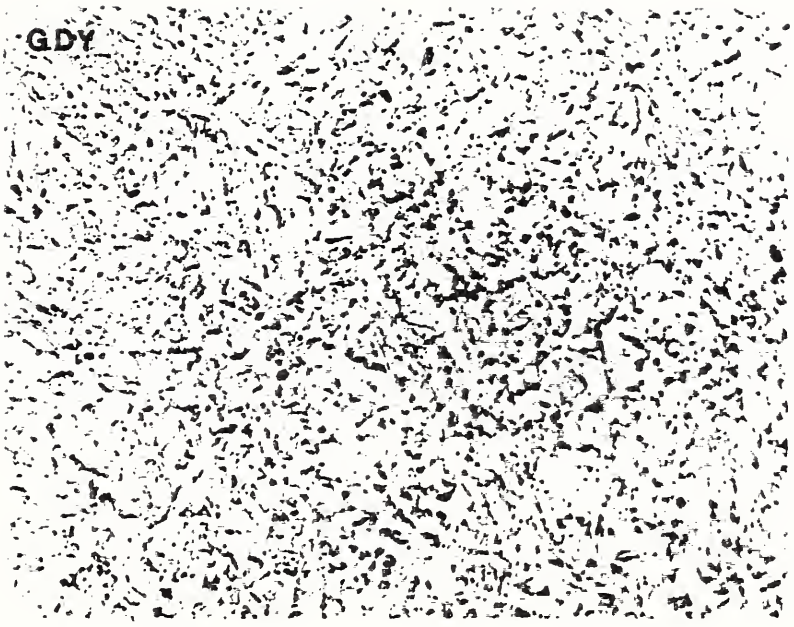

a

50 μm

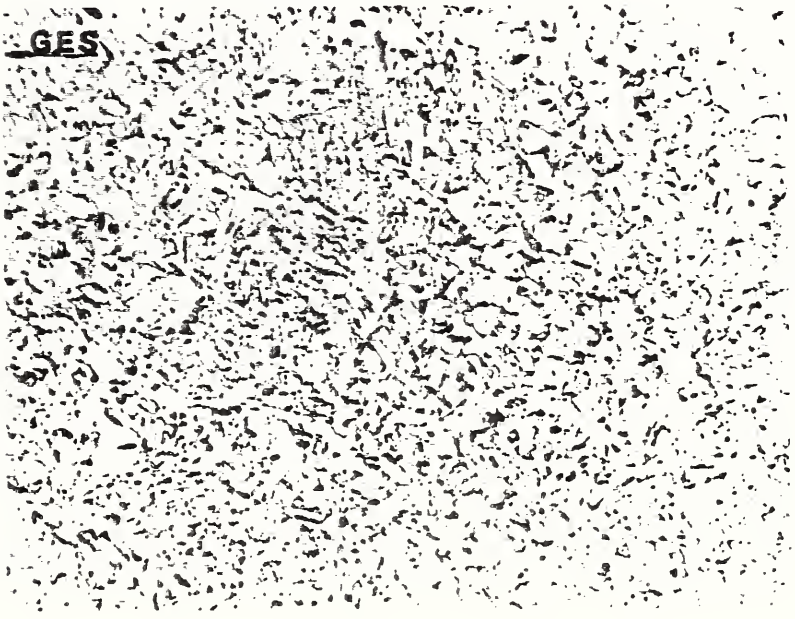

b

Figure 10. Light micrographs of samples from 1 in plates: a) GDY and b) GES. Both samples were etched in 2% nital; magnification is 500X; rolling direction is horizontal.

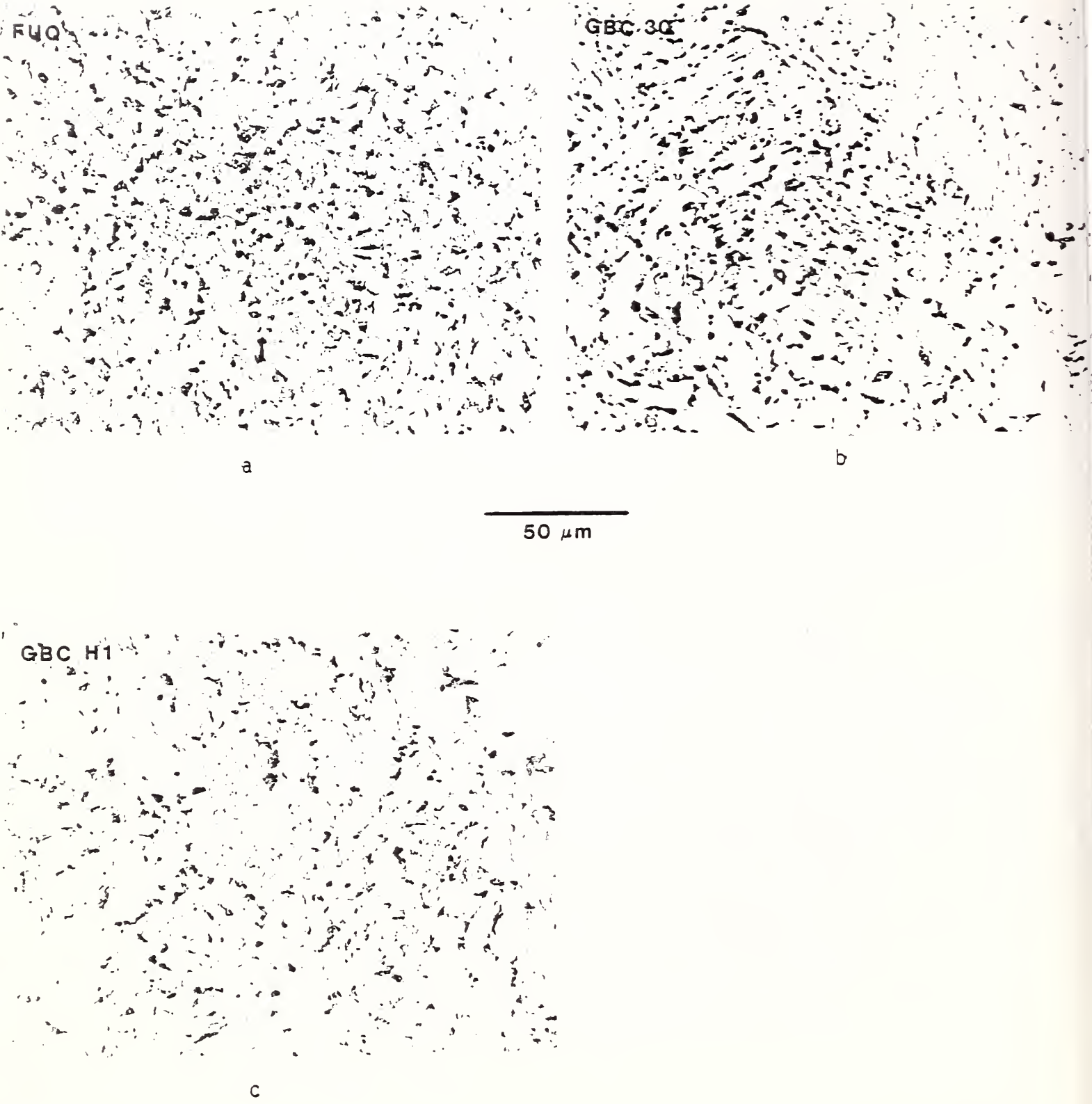

Figure 11. Light micrographs of samples from 1-1/4 in plates: a) FUQ, b) GBC-30 and c) GBC-H1. All samples were eteched in 2% nital; magnification is 500X; rolling direction is horizontal.

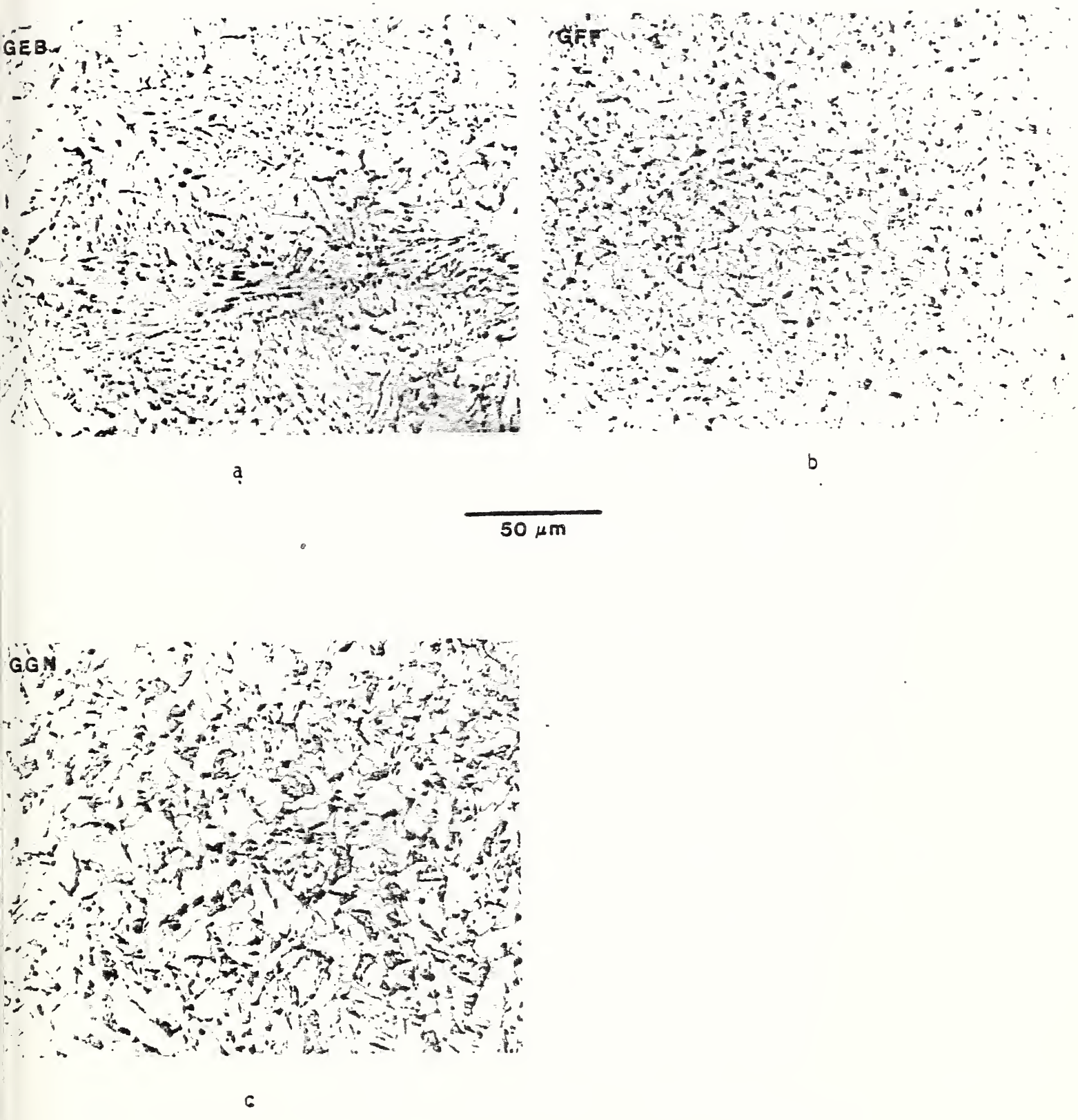

Figure 12. Light micrographs of samples from 2 in plates: a) GEB, b) GFF, and c) GGN. All samples were etched in 2% nital; magnification is 500X; rolling direction is horizontal.

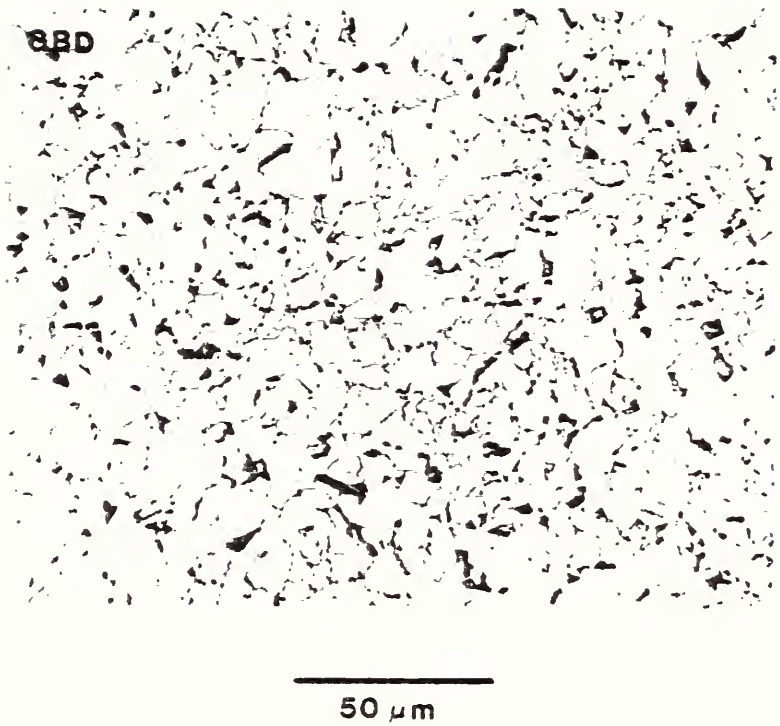

Figure 13. Light micrograph of a sample from 2-1/2 plate, GBD. The sample was etched in 2% nital; magnification is 500X; rolling direction is horizontal.

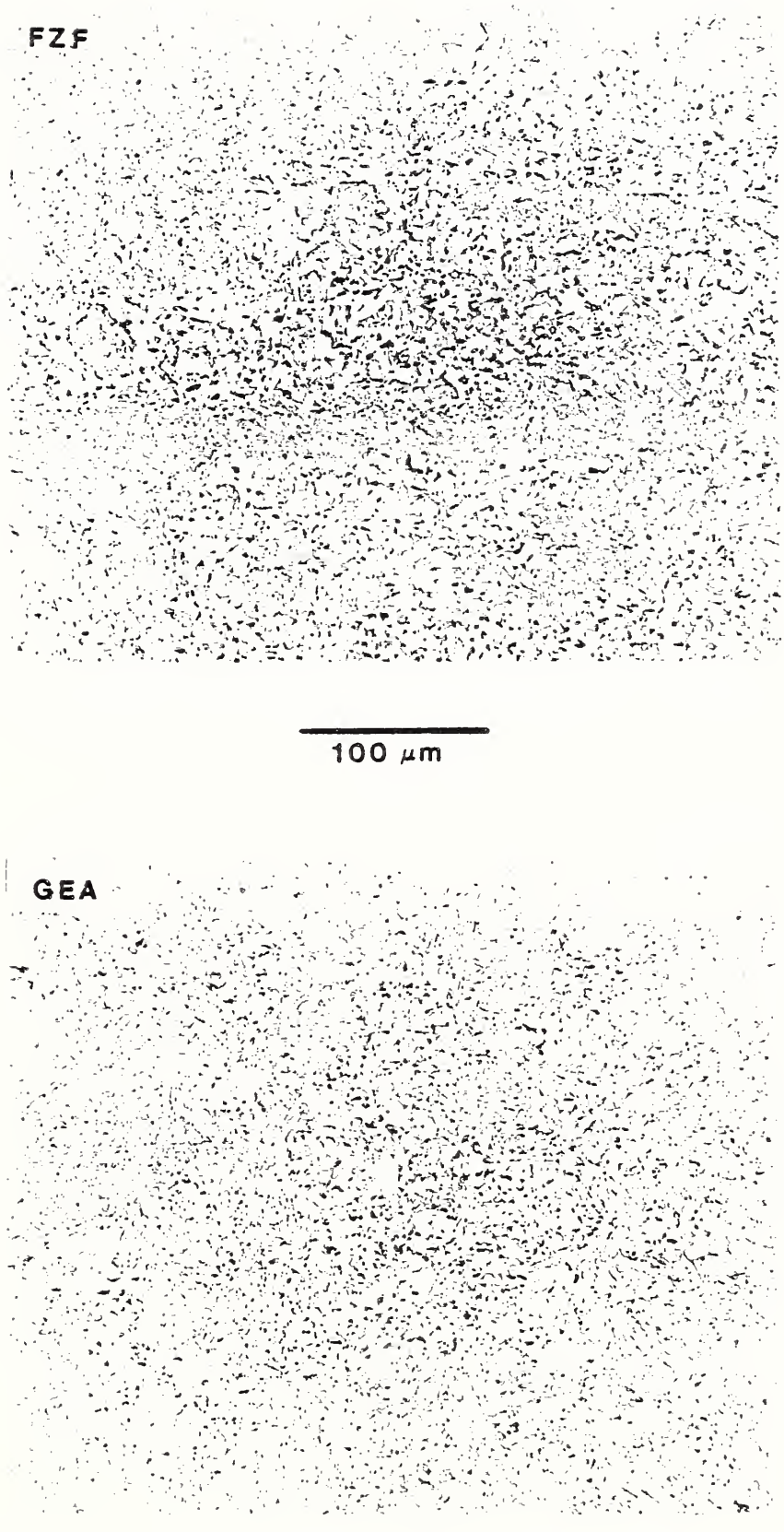

Figure 14. Light micrographs showing the microstructural banding in 3/4" plates: FZF (top) and GEA (bottom). Both samples were etched in 2% nital; magnification is 250X; rolling direction is horizontal.

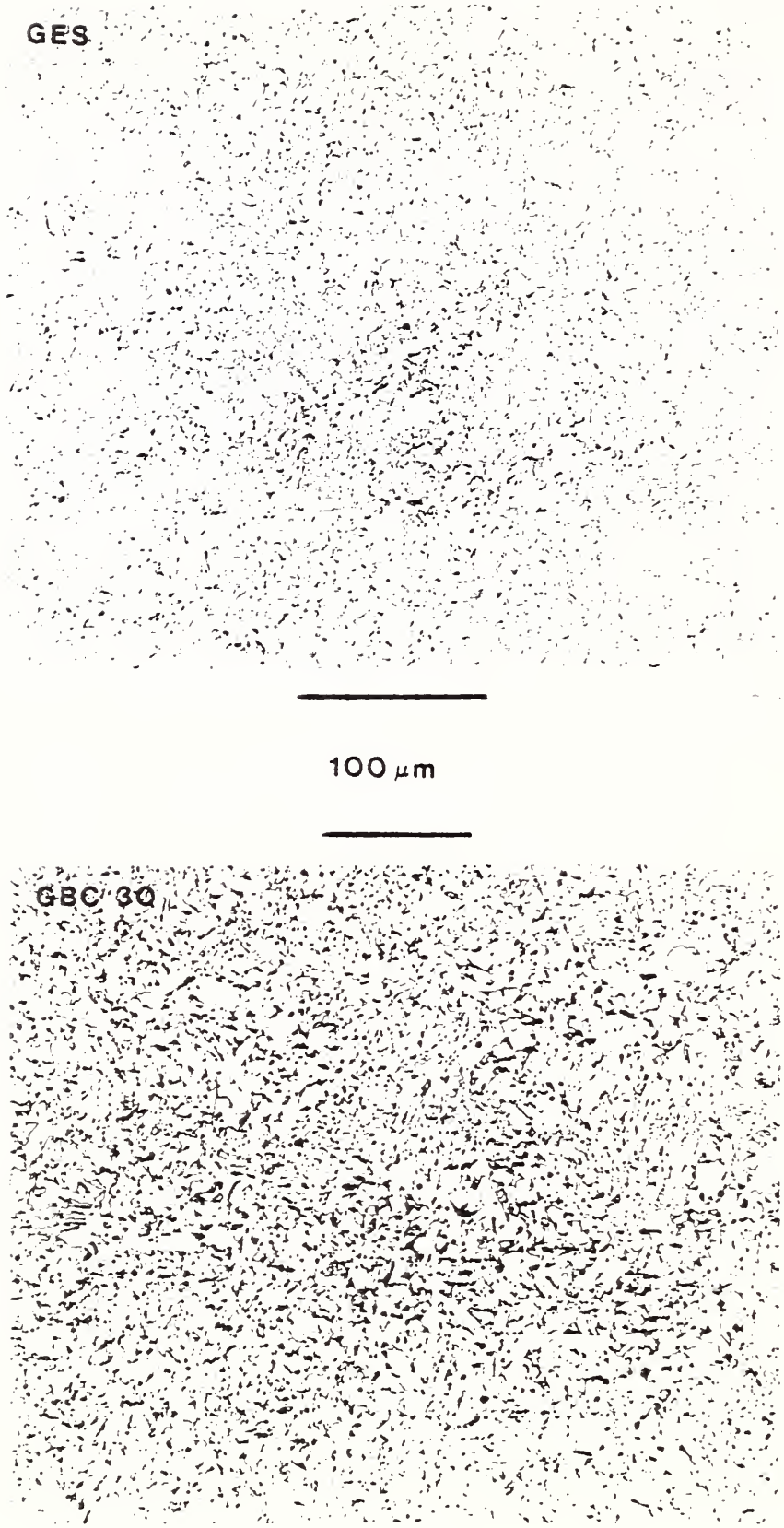

Figure 15. Light micrographs showing the non-uniformity of microstructure in 1 in and 1-1/4 in plates: GES (top) and GBC-30 (bottom), respectively. Both samples were etched in 2% nital; magnification is 250X on the top and 200X on the bottom; rolling direction is horizontal.

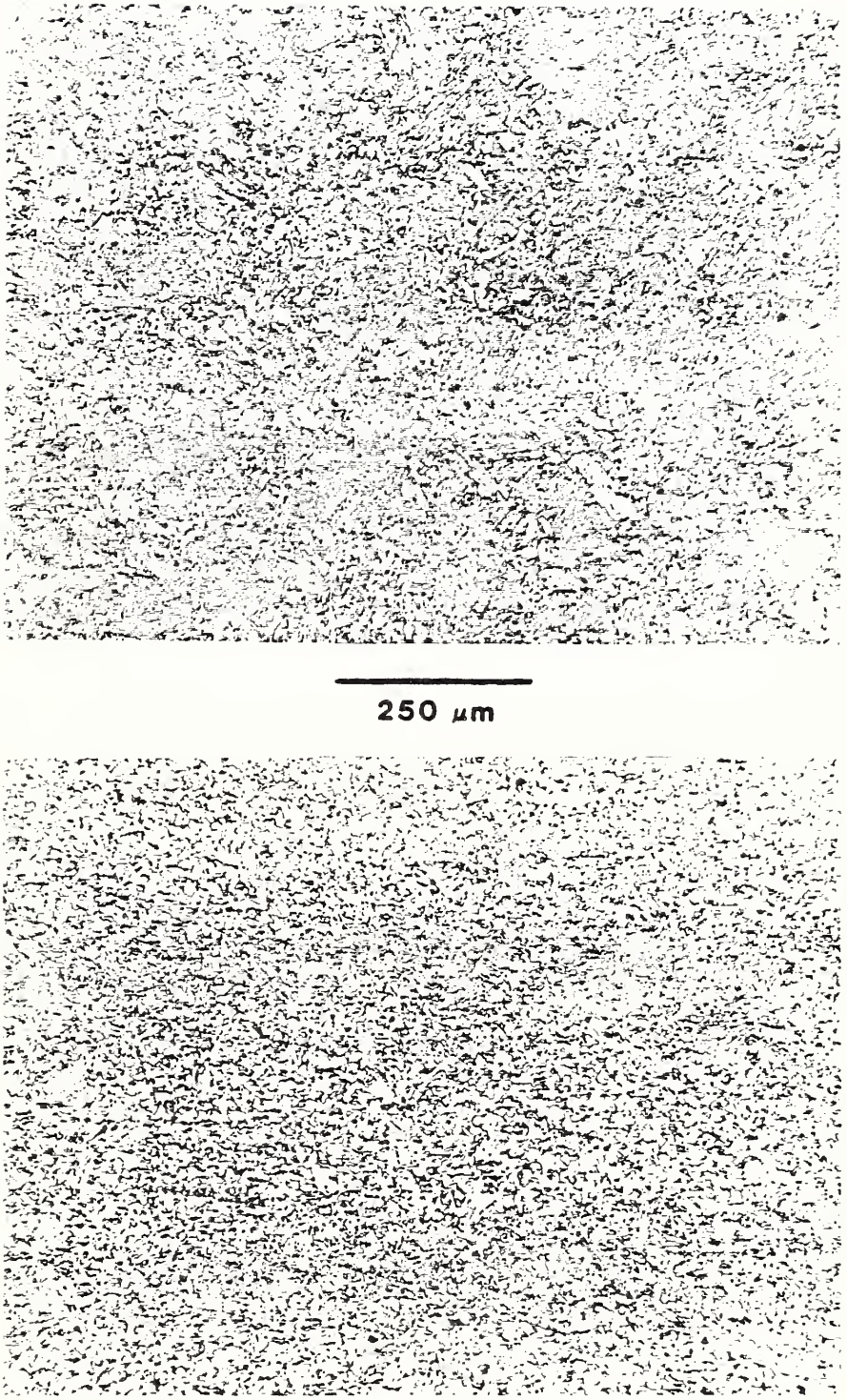

Figure 16. Light micrographs showing microstructural non-uniformity in 2 in steel plates: GEB (top) and GGN (bottom). Both samples were etched in 2% nital; magnification is 100X; rolling direction is horizontal.

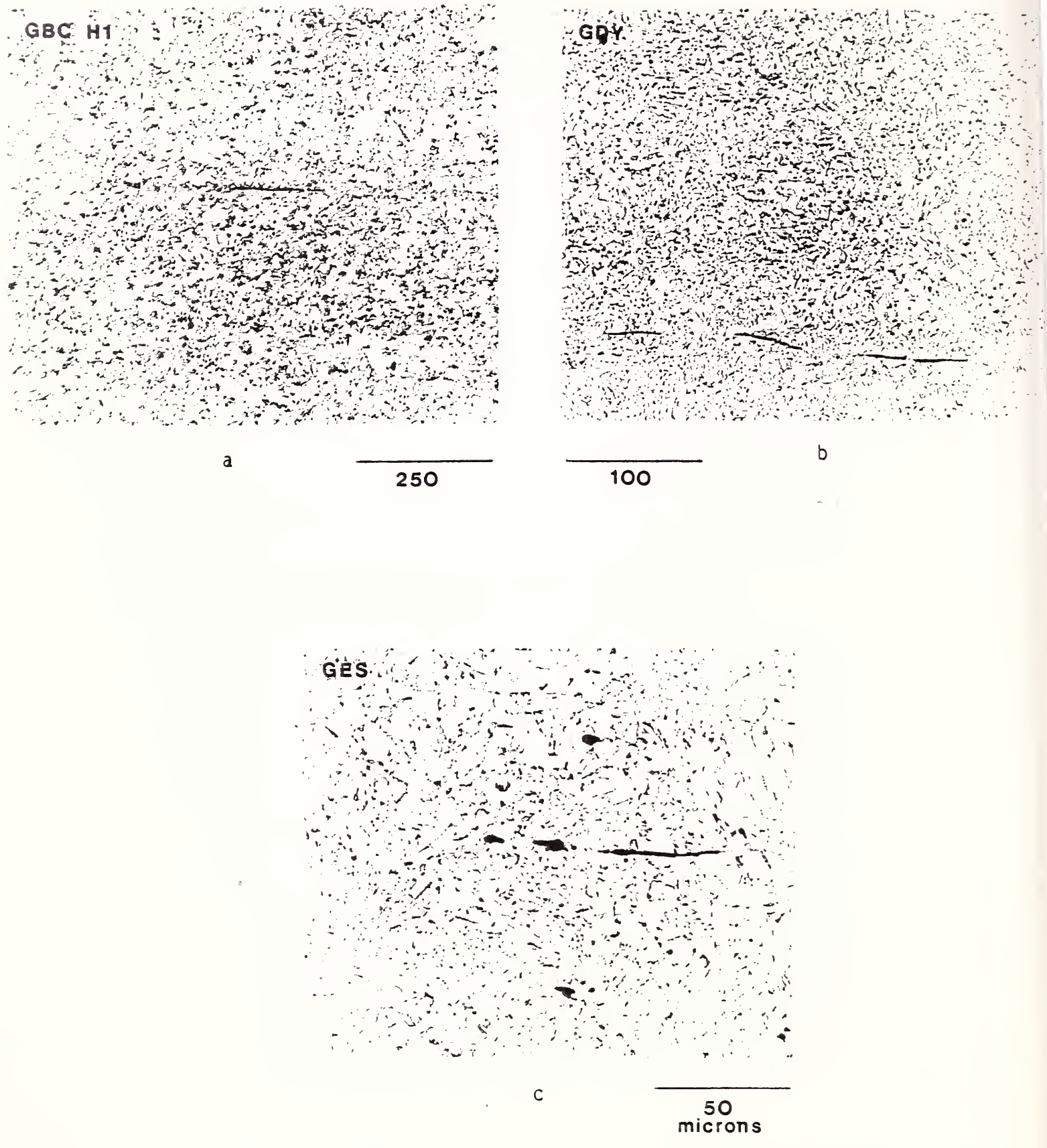

Figure 17. Micrographs showing the occurrence of elongated sulfides in "bainite streaks" in several plates: a) GBC, b) GDY, and c) GES. All samples were etched in 2% nital; rolling direction is horizontal.

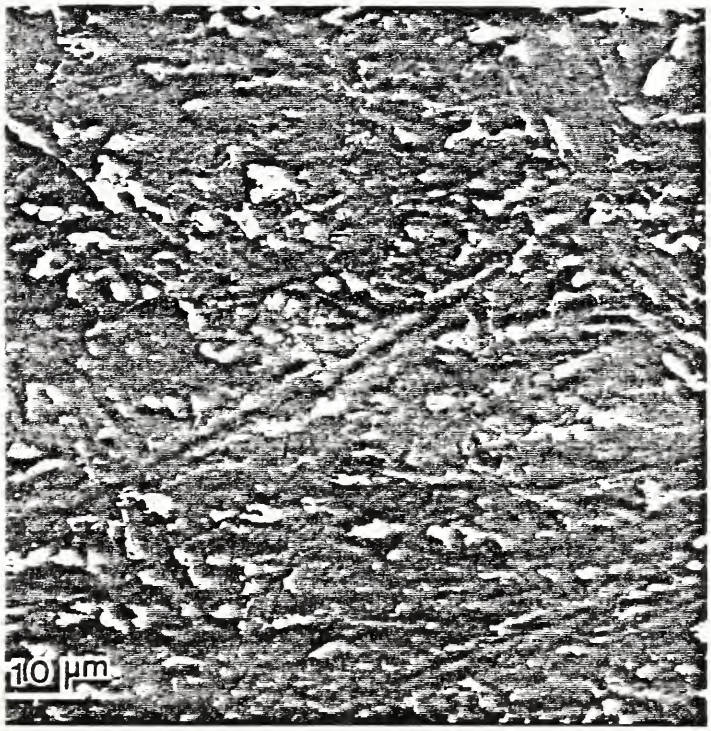

GEB

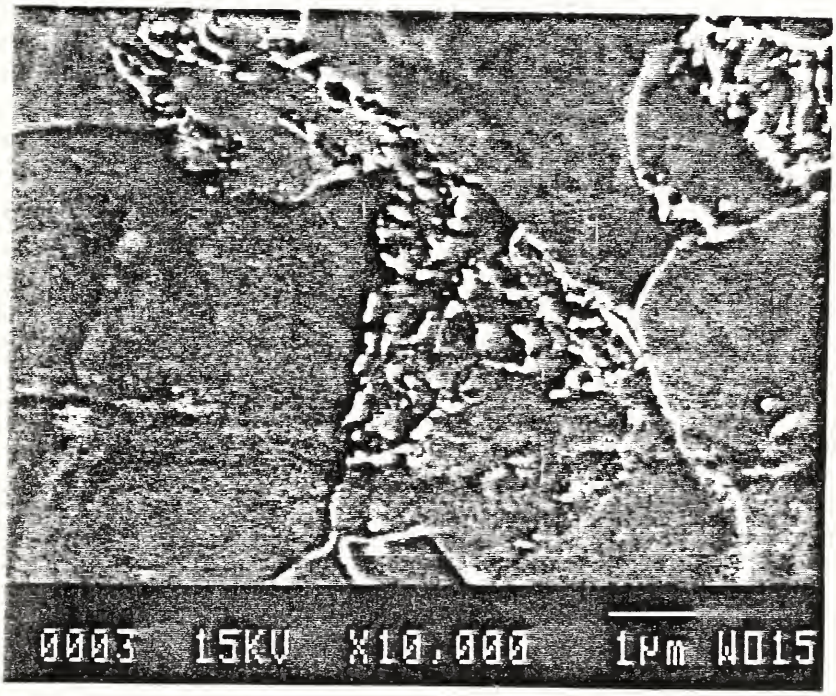

Figure 18. Scanning electron micrographs showing carbides in GEB. Sample was etched in HCl + picral.

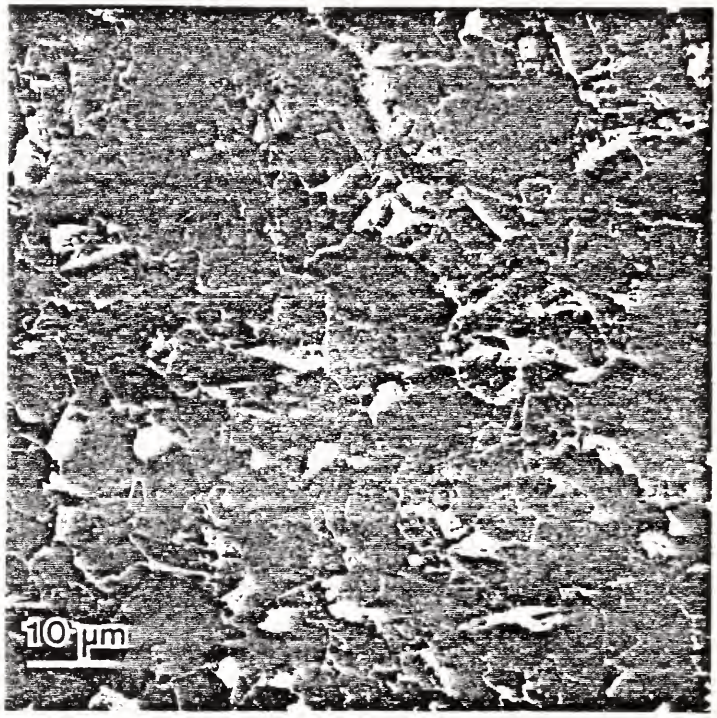

GBD

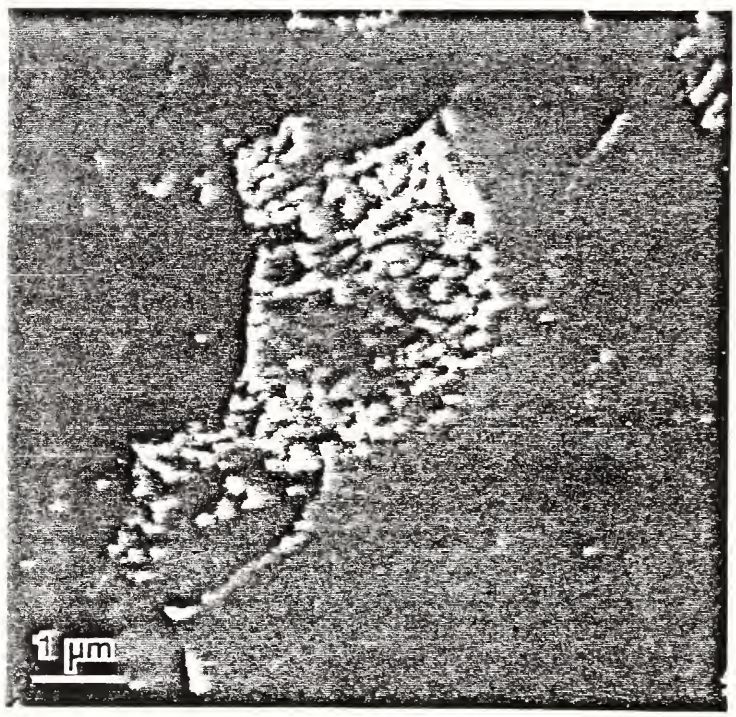

Figure 19. Scanning electron micrographs showing carbides in GBD. Sample was etched in HCl + picral and then in picral.

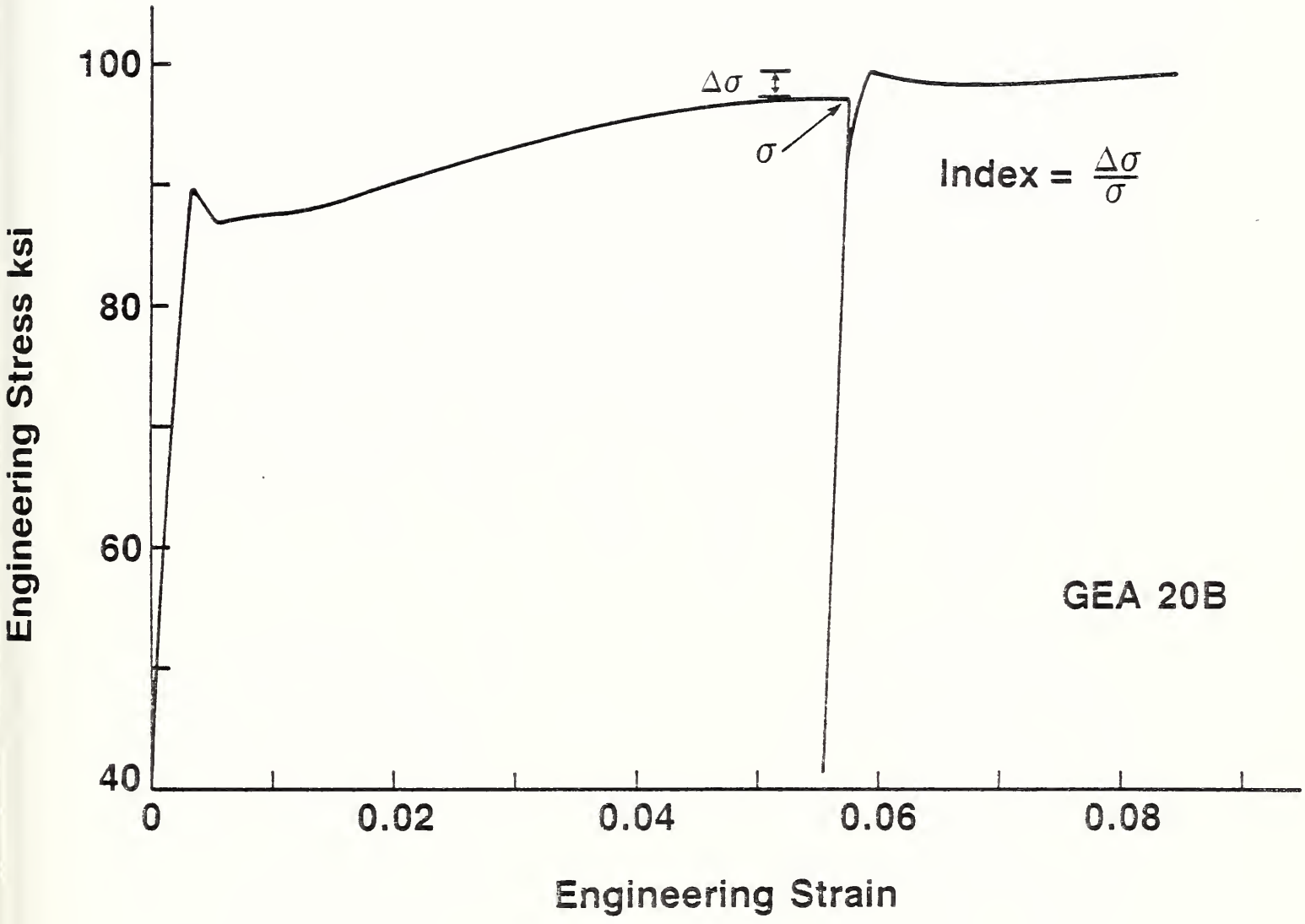

Figure 20. Engineering stress-strain curve from a strain aging test on s specimen from GEA20. The specimen was pulled up to the point marked σ, unloaded, aged at 100C for 1 hour and reloaded in tension. The strain aging index is given by $\Delta\sigma/\sigma$, as indicated.

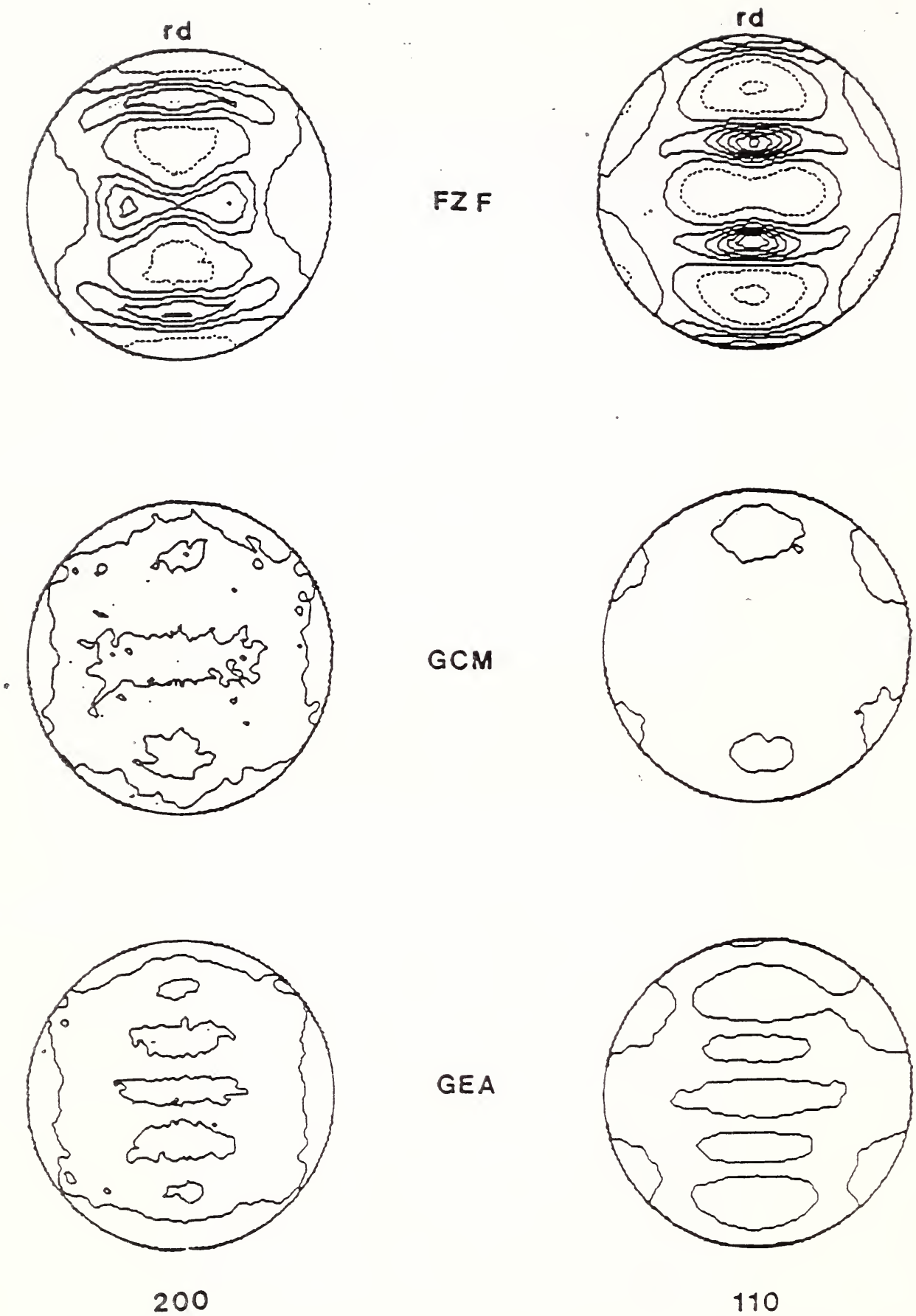

Figure 21. Neutron pole figures from 3/4 in plates: a) FZF, b) GCM, and c) GEA. The 200 pole figures are on the left; the 110 pole figures are on the right. The rolling direction is at the top of each figure.

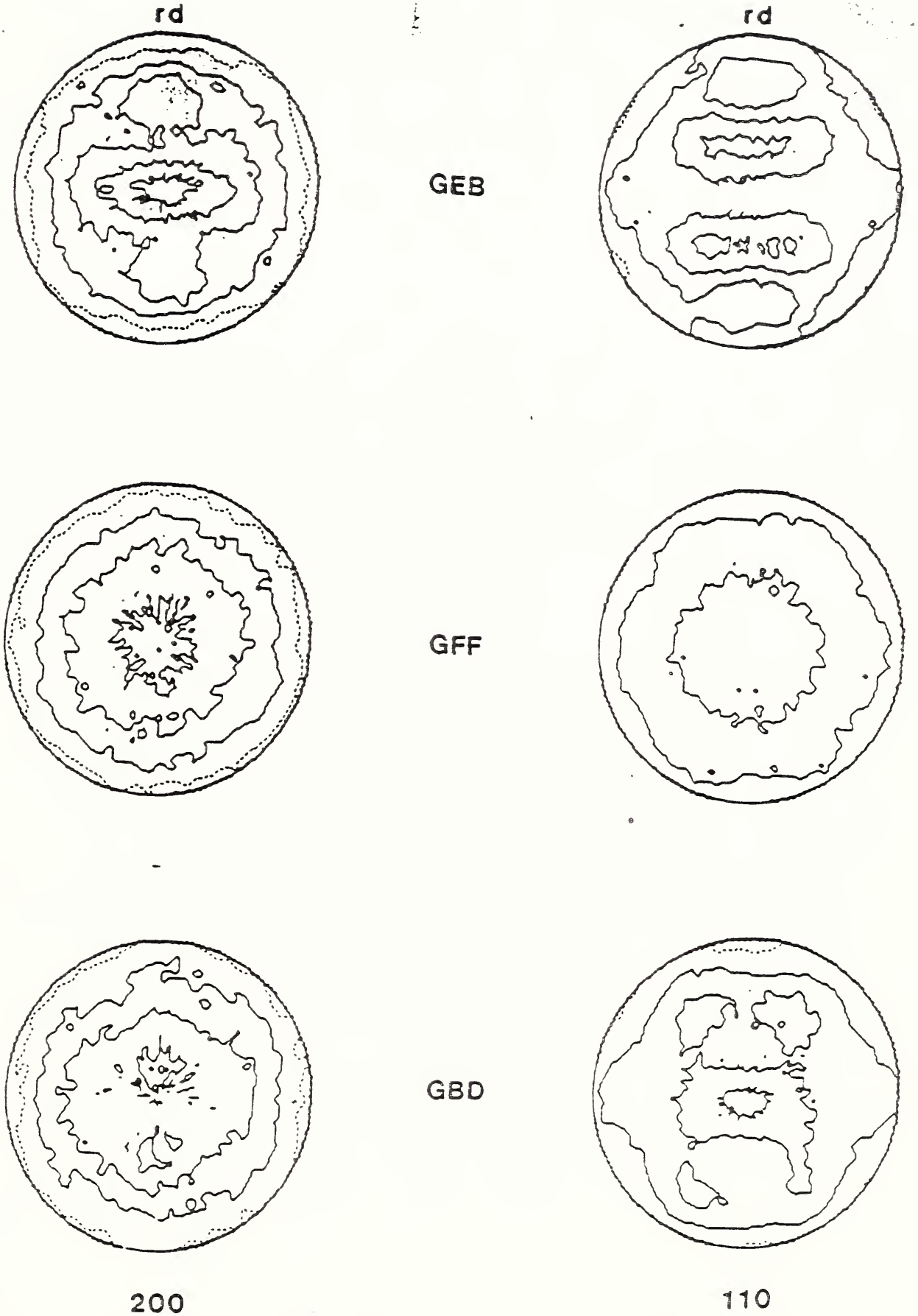

Figure 22. Neutron pole figures from 2 and 2-1/2 in plates: a) GEB, b) GFF, and c) GBD. The 200 pole figures are on the left; the 110 pole figures are on the right. The rolling direction is at the top of each figure.

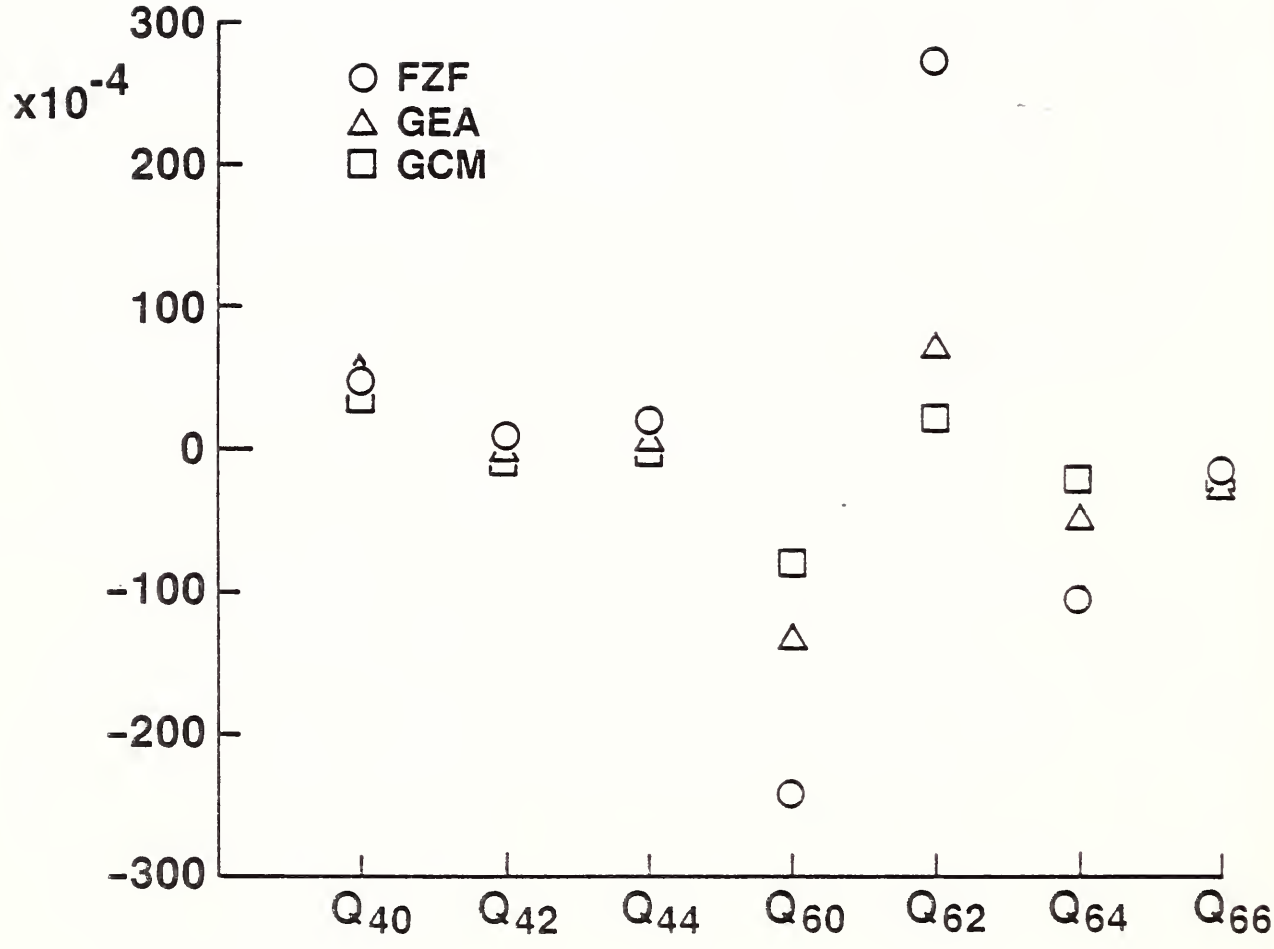

Figure 23. Values of $Q_{\ell m}$ for ℓ=4 and ℓ=6 from the (110) pole figures for the 3/4 in. plate specimens.

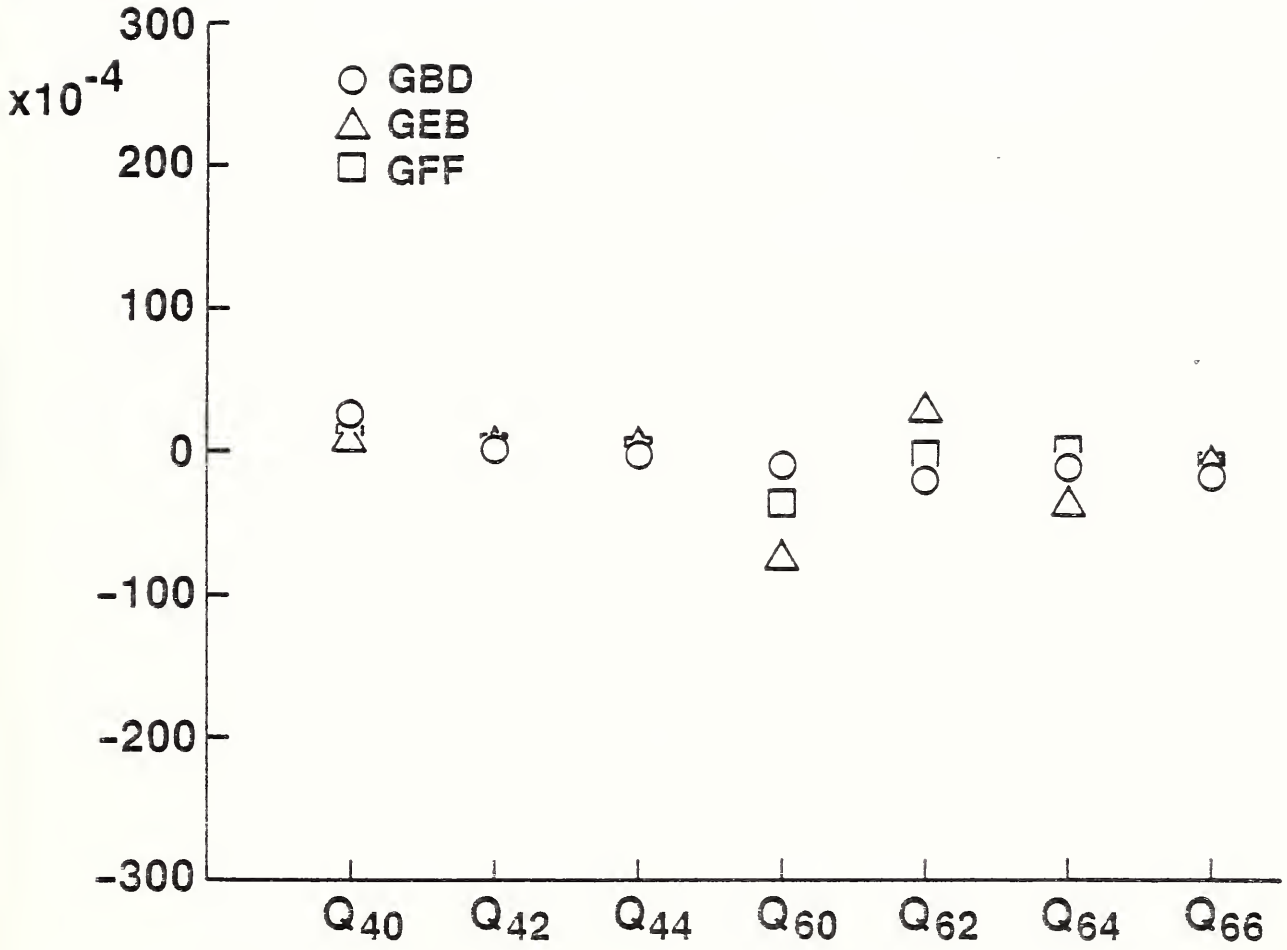

Figure 24. Values of $Q_{\ell m}$ for ℓ=4 and ℓ=6 from the (110) pole figures for the 2 and 2½ in. plate specimens.

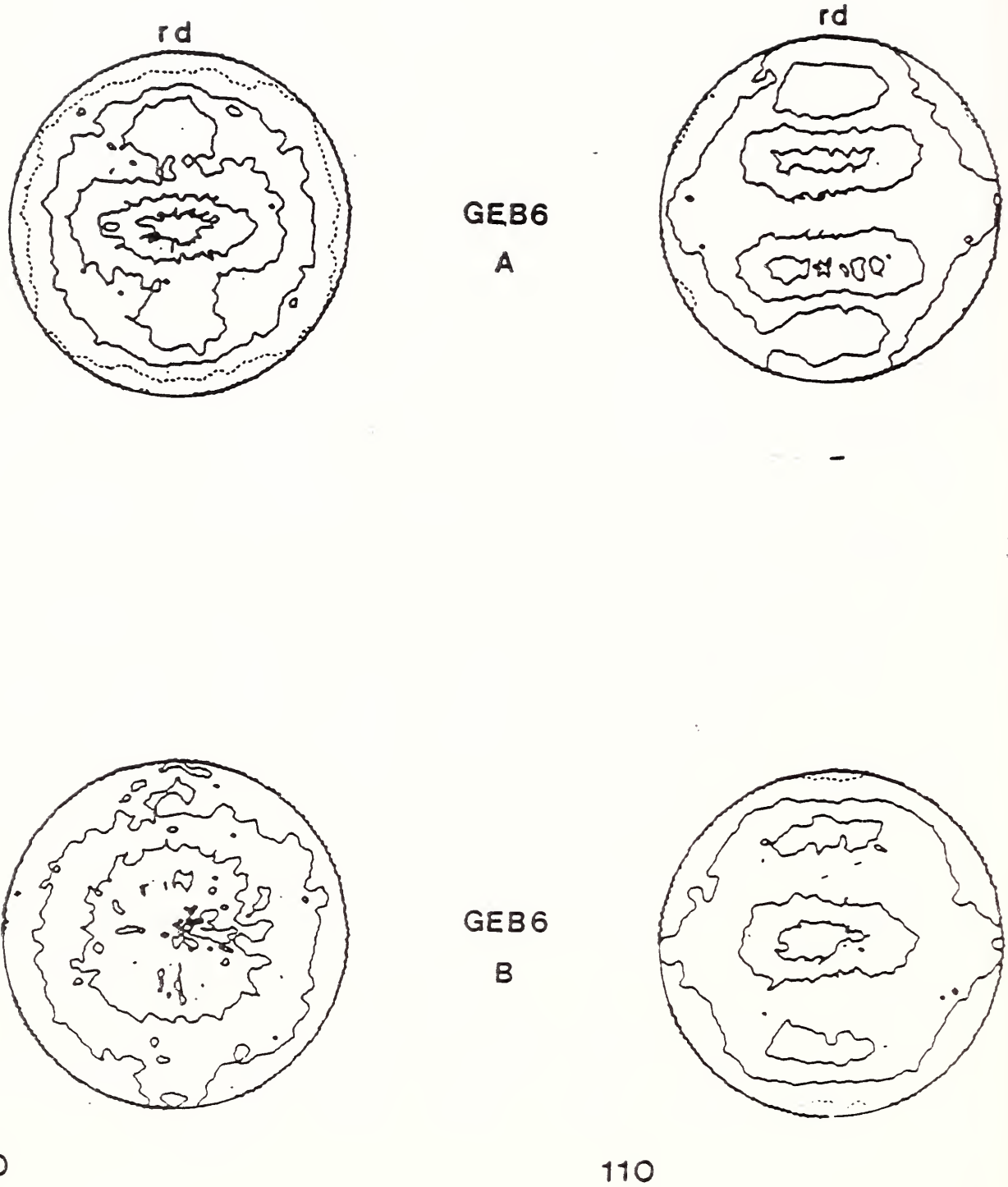

Figure 25. Neutron pole figures from opposite faces of the dynamic tear specimens GEB6. There may be stronger texture in the figures marked A; these are probably from the face that was closer to the center of the plate.

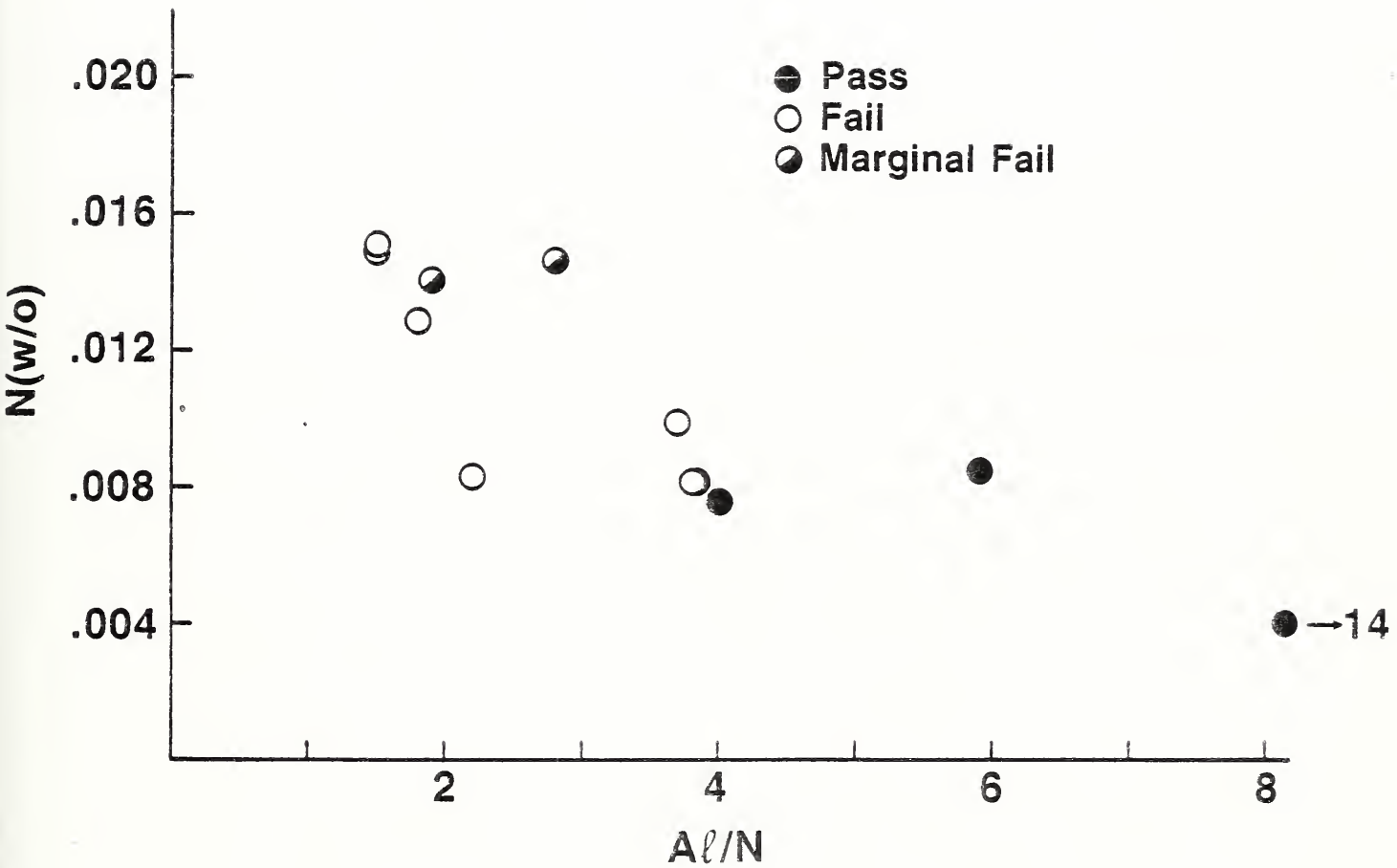

Figure 26. Explosion bulge test results - pass, fail, marginally fail - as they depend upon the N-content and the value of Al/N for each plate; these data are tabulation in Table VI.

NBS-114A (REV. 2-8C)

U.S. DEPT. OF COMM. BIBLIOGRAPHIC DATA SHEET (See instructions)	1. PUBLICATION OR REPORT NO. NBSIR 87-3647	2. Performing Organ. Report No.	3. Publication Date OCTOBER 1987

4. TITLE AND SUBTITLE

Microstructural Evaluation of Explosion Bulge Tested HSLA-80 Plates

5. AUTHOR(S)

M.J. Crooks, L.C. Smith, and R.C. Reno

6. PERFORMING ORGANIZATION (If joint or other than NBS, see instructions)

NATIONAL BUREAU OF STANDARDS
U.S. DEPARTMENT OF COMMERCE
GAITHERSBURG, MD 20899

7. Contract/Grant No.

8. Type of Report & Period Covered

9. SPONSORING ORGANIZATION NAME AND COMPLETE ADDRESS (Street, City, State, ZIP)

David Taylor Naval Ship R&D Center
Annapolis, Maryland

10. SUPPLEMENTARY NOTES

☐ Document describes a computer program; SF-185, FIPS Software Summary, is attached.

11. ABSTRACT (A 200-word or less factual summary of most significant information. If document includes a significant bibliography or literature survey, mention it here)

This work was undertaken to examine the microstructures of some HSLA-80 plates. The ultimate aim was to establish microstructural and chemical bases for variability in mechanical properties, in particular, behavior in explosion bulge tests. Steel chemistries, inclusion contents, ferrite microstructures, crystallographic textures and strain-aging responses were considered. The one variable that clearly distinguishes between plates that passed the bulge test and those that failed is the ratio of aluminum to nitrogen in the steel. For plates that passed, Al/N is 4 or greater. In plates with lower Al/N values, the embrittling effects of interstitial nitrogen, which could be present in the heat affected zones of these specimens, is likely responsible for failure in the bulge test.

12. KEY WORDS (Six to twelve entries; alphabetical order; capitalize only proper names; and separate key words by semicolons)

composition effects; inclusions; mechanical properties; microstructure; microstructure; steel; strain-aging; texture

13. AVAILABILITY

☐ Unlimited

☒ For Official Distribution. Do Not Release to NTIS

☐ Order From Superintendent of Documents, U.S. Government Printing Office, Washington, D.C. 20402.

☐ Order From National Technical Information Service (NTIS), Springfield, VA. 22161

14. NO. OF PRINTED PAGES

15. Price